國立交通大學

光電工程研究所

博 士 論 文

緊束縛理論在光子晶體波導的應用

Tight Binding Theory for Photonic Crystal Waveguides

研 究 生：黃至賢

指導教授： 謝文峰 教授

中 華 民 國 九 十 八 年 六 月

緊束縛理論在光子晶體波導的應用

Tight Binding Theory for Photonic Crystal Waveguides

研究生：黃至賢   Student: Chih-Hsien Huang

指導教授：謝文峰 教授   Advisor: Prof. Wen-Feng Hsieh

國立交通大學

光電工程研究所

博士論文

A Dissertation Submitted to

Department of Photonics and Institute of Electro-Optical Engineering

College of Electrical and Computer Engineering

National Chiao Tung University

in Partial Fulfillment of the Requirements

for the Degree of Doctor of Philosophy

in

Electro-Optical Engineering

June 2009

Hsinchu, Taiwan, Republic of China

中華民國九十八年六月

緊束縛理論在光子晶體波導的應用

研究生: 黃至賢   指導教授: 謝文峰　教授

國立交通大學光電工程研究所

摘要

　　本論文利用緊束縛理論來研究脈衝在單一且非線性光子晶體波導或共振耦合波導以及電磁波在對稱或非對稱線性光子晶體耦合波導的傳播情形。從考慮缺陷間耦合的緊束縛理論，電場在光子晶體和共振耦合波導的振幅可以寫成一個解析演化方程式，此方程式稱為延伸離散非線性薛丁格方程式。在光子晶體波導或共振耦合波導中，藉由解這個方程式我們可以得到光調制不穩定區域及在不同的平面波向量(p)和不同擾動波向量(q)的增益係數G(p,q)的解析解形式。在共振耦合波導中，光調變不穩定的區域只能出現在pa大於π/2或者小於π/2中。這裡a指的是缺陷間的距離。而光調變不穩定區域的位置會由缺陷間界電柱數目以及克爾係數的正負號所決定。然而，在光子晶體波導中，光調變不穩定區域中的pa可以超過π/2。當平面波的相位pa超過π/2，在固定pa的情況下，光調變不穩定區域的增益曲線G(q)會有兩個最大值，這和非線性光纖中的情況有很大的不同。

　　另外一方面，我們也成功地利用延伸離散非線性薛丁格方程式來描述光固子在含有克爾介質的非線性光子晶體波導及共振耦合波導中的傳播及其傳播的條件。從這個條件，我們得到了光固子在不同數目的間隔界電柱及不同自相位調變強度下的穩定傳播區域，這和光調變不穩定區域是吻合的。光子晶體波導中，在低頻或者低

波向量的脈衝傳播時，需要加入正的克爾係數的物質到波導中，反之亦然。由於光子晶體波導和共振耦合波導的耦合係數大小不同，導致共振耦合波導的群速度、色散和支持光固子傳播的自聚焦強度比光子晶體波導小。對於一個長脈衝在光固子傳播條件下，他的脈衝擴散由於大於二階的的最低階色散係數所造成。當脈衝變窄，其他高階項需要被考慮，這導致光固子最小擴散的自聚焦強度會比導出來的傳播條件小，尤其在三階色散趨近於0的時候更加明顯。

當另一個相同的波導刻入光子晶體中且與原波導相隔一排或數排介電柱，我們可以得到一個光子晶體耦合器。耦合器的色散曲線會有一個交點，稱為不耦合點。在這個點上，能量不能耦合到另一個波導。所以我們可以利用調變不耦合點來改變耦合器的性質。從考慮到兩個波導間的耦合到次鄰近缺陷的緊束縛理論，我們發現如果平行於耦合器的方向去移動缺陷柱，不耦合點頻率在正方晶格會有藍移的現象，但在三角晶格則有紅移的現象。如果讓缺陷互相靠近，由於耦合強度變強，導致耦合器的傳播頻率及兩條色散曲線間的頻率差都有增加的趨勢。當我們利用平面波展開法及時域有限差分法來作模擬時，發現其結果跟我們的理論非常吻合。

如果光子晶體中的兩條波導不一樣，耦合器變的不對稱。利用考慮到兩個波導間的耦合到次鄰近缺陷的緊束縛理論，我們解釋了幾個非對稱耦合波導的物理性質:(1)在某個特定點時，耦合波導的色散曲線會退化到單一波導的色散曲線且電場只會侷限在單一個波導中，此點我們稱為不耦合點;(2)即使色散曲線沒交叉，本徵模態的宇稱仍會在不耦合點交換;(3)即使本徵模態交換，高頻色散曲線的電場會主要分佈在擁有較高本徵模態的單一波導，反之亦然。當一個單頻光射入耦合器中，能量的轉換也可以用解析解的形式表達。由於色散曲線沒交叉，所以在非對稱的耦合波導的耦合長度並非無限大，但是在不耦合點兩個波導間有最低的能量轉換。

Tight binding theory for photonic crystal waveguides

Student: Chih-hsien Huang   Advisor: Dr. Wen-Feng Hsieh

Department of Photonics & Institute of Electro-Optical Engineering

National Chiao Tung University

Abstract

Tight binding theory (TBT) is used to study the pulse propagation in singe photonic crystal waveguides (PCWs) and coupled resonant optical waveguides (CROWs) with nonlinear media as well as an electromagnetic (EM) wave propagation in the symmetric and asymmetric photonic crystal (PC) coupler.   From the TBT and considering the coupling between the defects, the amplitude of the electric field in the PCWs or CROWs can be expressed as an analytic evolution equation and we termed it the extended discrete nonlinear Schrödinger (EDNLS) equation.   By solving this equation for CROWs and PCWs, we obtained the modulation instability (MI) region and the MI gains, $G(p,q)$, for different wavevectors of the incident plane wave (p) and perturbation (q) analytically. In CROWs, the MI region, in which solitons can be formed, can only occur for pa being located either before or after $\pi/2$, where a is the separation of the cavities.   The location of the MI region is determined by the number of the separation rods between defects and the sign of the Kerr coefficient.   However, in the PCWs, pa in the MI region can exceed the $\pi/2$.   For those wavevectors close to $\pi/2$, the MI profile, $G(q)$, can possess two gain

maxima at fixed *pa*. It is quite different from the results of the nonlinear CROWs and optical fibers.

We also successfully used the EDNLS equation to describe the soliton propagation and to obtain the soliton propagation criteria (SPC) in the nonlinear PCWs and CROWs containing Kerr media. From these criteria, we obtained the soliton propagating region of CROWs in different numbers of separated rods and strengths of self-phase modulation which coincides with the region of MI of the CROWs. In the PCWs, the positive Kerr coefficient medium needs to be added to support the pulse propagation in the low frequency or wave vector region of the dispersion relation and vice versa. Due to the different magnitudes of coupling coefficients in CROWs and PCWs, the group velocity, dispersion and self phase modulation strength to support soliton propagation in CROWs are smaller than those in PCWs. For a long pulse, only the lowest nonzero dispersion coefficients, β_n with $n > 2$ needs to take into consideration for pulse broadening at the SPC. However, as decreasing the pulse width, even higher order dispersion should be taken into account that makes the self phase modulation strength smaller than the criteria when the third order dispersion is almost zero.

As the other identical waveguides is inserted into the PC with one or several partition rods, the PC coupler is created. The dispersion relation curves of the coupler could be crossing. The crossing point is named as the decupling point. At this point, the energy cannot be transfer into the other waveguide. Controlling the decoupling point can modify the properties of the coupler. From the TBT that includes coupling of the guiding mode field up to the next nearest-neighbor defects, we find there is a blue shift in the frequency of the decoupling point in the square lattice and red shift in the triangular lattice by translating the defect rods along the axis of the coupler. By moving defects of

the coupler close to each other transversely, not only the eigenfrequencies of the coupler but also separations of dispersion curves increase due to the stronger coupling between defect rods. From the simulation results of the plane wave expansion method and finite difference time domain method, the theoretical analysis of TBT gets a great agreement with the numerical ones.
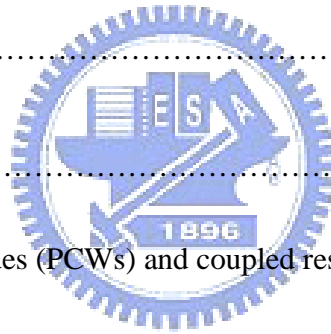
If the other waveguide inserted into the PC is different from the original one, the coupler will be asymmetric. By considering the next nearest-neighbor defects between two PCWs, analytic formulas derived by the TBT, we will explain the physical properties of the asymmetric directional coupler made of two coupled PCWs: (1) The dispersion curves of a PC coupler will decouple into the dispersion curves of a single line defect, and the electric field would only be localized in one waveguide of the coupler at a particular point that we name the decoupling point; (2) The parities of the eigenmode switch at the decoupling point, even though the dispersion curves are not crossing; (3) The eigenfield at a higher (lower) dispersion curve is always mainly localized in the waveguides that have higher (lower) eigenfrequencies of single line defects, even though the eigenmodes are switched. As a given frequency is incident into the coupler, the energy transfer between two waveguides and the coupling length can be expressed analytically. Due to no dispersion curve crossing, the coupling length is no longer infinite at the decoupling point in asymmetric PCWs, but it still possesses the minimal energy transfer between two waveguides when the frequency of the incident wave is close to the decoupling point.
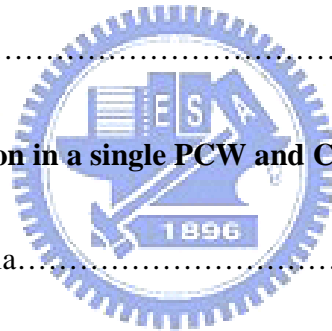
Acknowledgement

Contents

List of Figures

x

List of Tables

Chapter 1 Introduction

1.1 Photonic crystals

Photonic crystals (PCs) arise from the cooperation of periodic scatters thus, they are called "crystal" because of their periodicity and "photonic" because of their action on light [1]. The concept behind these materials stems from pioneering work of Yablonovitch and John [2-6]. Yablonovitch proposed a structure in which an electronic and photonic gap overlapped, making it possible to enhance the performance of lasers, heterojunctions, bipolar transistors, and solar cells [4]. In the same year, John also proposed using such structures for the localization of light in strongly scattering dielectric structures [3]. A PC is interesting owing to whose band structure possesses a complete photonic band gap (PBG) [5-7]. A PBG defines a range of frequencies in which light cannot propagate inside the crystals. As a result of the existence of PBGs and their unusual dispersion properties, photonic crystals can sustain various light waves, pulses, and beam propagation regimes which are of physical interest and important for numerous applications, such as perfect reflector and negative refraction index structures.

The mathematic description of the PCs should start from the four Maxwell's equations rather than other scalar wave description, such as the beam propagation method, because the special variation of the refraction index is comparable to the wavelength. From the researches in early 1990s, four main algorithms are proposed to model the wave propagation in the PCs. They are the plane wave expansion method (PWEM) [8, 9], finite difference time domain (FDTD) method [10-12], finite element method (FEM) [13, 14] and transfer matrix method (TMM) [15, 16]. The PWEM deals with the Maxwell's

equations in wave vector space and solves the eigenfrequencies in each wave vector to get the dispersion relation. It is suitable for the high periodic structures. In the FDTD method, a wave propagating through the PC structure is found by a direct discretization of Maxwell's equations in both time and space. It is powerful and flexible especially in a complex structure but is extremely time-consuming and its computational requirements grow exponentially with problem size. The FEM is a frequency domain method used to solve Maxwell's equations. It takes into account material discontinuities in the dielectric structure more efficiently by a preconditioned subspace iteration algorithm, which helps overcome the slow convergence of the PWEM. It is widely used to simulate the dispersion of the photonic crystal fiber due to its structure uniformity in the wave propagation direction. TMM is powerful at layer structures such as 1D PCs or 2D and 3D PCs with square lattices. A matrix is used to connect the electric field or magnetic field between two layers. By solving the matrix, the transmission, refraction and dispersion relation can be obtained.
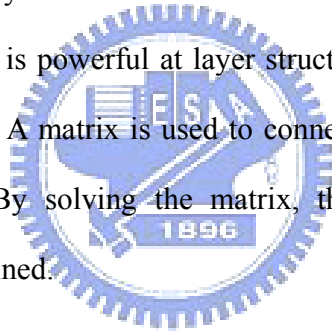
1.2 Photonic crystal waveguides and coupled resonant optical waveguides

A photonic crystal waveguide (PCW) can be created by sequentially changing the radius or dielectric constant of the dielectric rods or changing the radius of periodic air holes in a dielectric slab; on the other hand, the coupled resonator optical waveguide (CROW) is created by arranging the cavities, made of point defects, periodically [17, 18]. The electromagnetic (EM) wave can propagate in these channels, PCWs or CROWs, with a very low loss even through a sharp bend [19]. Combining the point defects with the

PCWs or CROWs can be used to modulate the wave [20-22]. Lots of researches were focused on design the structures to modulate light to realize the all optical devices such as (1) Waveguide crossings: The perpendicular crossings in the waveguides intersection exhibit negligible crosstalk which closes to 10% when the waveguide width is on the order of a wavelength. The design in PC waveguide permitting single-mode waveguides with optimal miniaturization falls as low as 10^{-9} [23]. (2) Waveguide branches: An idea waveguide branches is a device that splits the input power into two or more output waveguides without significant reflection or radiation losses [24, 25]. (3) Channel drop filters: Channel dropping filters are devices that are necessary for the manipulation of wavelength division multiplexing optical communications [26]. PCs present a unique opportunity to investigate the possibilities of miniaturizing such a device to the scale of the wavelength of interest.

These defect resonators in the CROWs are designed such that their resonant frequency falls within the band gap of the surrounding 2D structure, which permits high-Q optical modes and the coupling is due to the overlap of evanescent waves between two cavities [17]. Therefore, the energy is strong localized in the cavities with very low group velocity. If nonlinear media are added in the cavities, the high Q and slow light in the CROWs will enhance the nonlinearity of the media. Another appearing feature of the CROW is the possibility of making lossless bends. Since the coupling of the corner resonator to its two immediate neighbors is identical due to its rotational symmetry, the transmission coefficient through the bend is 100% throughout the entire CROW band. That is contract with the PCWs, 100% transmission occurs only at a particular frequency [19].

1.3 Photonic crystal coupler

The photonic crystal coupler is formed by two adjacent PCWs with one or several row(s) of partition rods [27, 28]. When we calculate the dispersion relation of this structure of two identical PCWs, there would be two dispersion relation curves existed within the band gap [29, 30]. One is odd mode and the other is even mode [29]. An EM wave with a given frequency located on the dispersion curves is incident into one channel (PCW) of this coupler will couple into the other channel. The coupling length, in which the EM wave completely or maximally couples into the other waveguides for the symmetric or asymmetric cases, is defined as $\pi/\Delta k$, where Δk is the wave vector mismatch between two modes at the given frequency. The coupling length highly depends upon the incident frequency that can be used to design the demultiplexer [30-32]. The directional coupler can also be used to design power splitter [33], polarization splitter [34] and add/drop filters [35]. If a nonlinear medium is added in the branch of the waveguides, the switch which is controlled by the EM wave or the external electric field can also be fabricated by directional coupler structures [36].

1.4 Motivations

The tight binding theory (TBT) has been widely used in the CROWs to describe the amplitude of the EM wave propagation in linear or nonlinear system. When a plane wave is incident in these structures, the dispersion of the CROWs can be obtained by PWEM. The numbers of the separation rods extremely influence the sign and the slope of dispersion relation. From the dispersion relation, we can derive the group velocity and various orders of the group velocity dispersion (GVD) which means the difference of the separation rods in the CROWs will also determine the sign and the magnitudes of the

4

group velocity and GVD. Once, the nonlinear material is added in the waveguides region, the dispersion relation curve of the CROW has a constant frequency shift comparing to the curve of linear waveguides, so the linearly physical properties of the waveguides will be preserved and the properties will influence the performance of the nonlinear materials. Therefore, the properties of the CROWs with different separation rods or structures should initially be investigated and the TBT provides a powerful method for us to realize these properties.

As the defect rods are made of nonlinear materials such as Kerr media, the perturbation superimposed on a plane wave could grow exponentially at a certain condition. It is named as the modulation instability (MI). Because the field evolution in the PCWs with Kerr media can be expressed as a discrete nonlinear Schrödinger (DNLS) equation, the MI region and gain can be derived from this equation. On the other hand, when a pulse is incident into the waveguides with nonlinear materials, the pulse could propagate in the waveguides without distortion which is the so-called soliton. The criterion for soliton propagation under slowly varying envelope approximation (SVEA) can also be derived by the DNLS equation. Therefore, we can use this criterion to discuss the soliton propagation regions in different structures of CROWs. When the width of the pulse becomes shorter, the SVEA is broken. The soliton disperses under propagation due to the high order GVD. We can take the Fourier transform of the amplitudes of the pulse to discuss the pulse broadening caused by high order GVD under soliton propagation condition.

In PCWs, the distance between two defect rods (a) is so close that the next nearest-neighbor coupling is no longer negligible. Under this circumstance, the evolution equation to describe the wave propagation in the PCWs with nonlinear material

5

should be written as an extended formula.   In general, the next nearest-neighbor coupling coefficient is approximately one order smaller than the nearest-neighbor coupling coefficient, such making the properties in the PCWs is different from the properties in the CROWs especially when ka = π/2.   Therefore, it is needed to take advanced discussion on the MI and soliton propagation in the PCWs.

When the other identical waveguide is carved into PCs and partitioned with one or several rows of perfect rod(s), another useful device, the directional coupler (DC), is created.   The dispersion relation curve of the coupler is usually crossing with triangular lattice but rare crossing in the square lattice.   This phenomenon gives some limitation as designing the device.   Therefore, we want to create the crossing point in the square lattice and then to move the crossing point at square lattice or triangular lattice which be achieved by moving the defect rods in the waveguides.   We also want to use TBT to further realize the trend of shift of the crossing point as moving the defect rods.

On the other hand, when the other waveguide is created asymmetrically, the dispersion relation calculated by PWEM would not cross anymore, but the parity of the eigen mode may switch at a particular point, in which point we named it the decoupling point.   At this point, the electric field is only localized at one waveguide of this asymmetric coupler. These phenomena cannot give a good explanation by the numerical simulation results. Therefore, we also want to use TBT to derive an analytic description to realize the physical properties of asymmetric PC couplers.

1.5 Organization of the dissertation

In this dissertation, we firstly use TBT to derive the electric field evolution equation in single PCWs and CROWs with or without the nonlinear media in Chapter two.   The

coupling equations of double PCWs and the properties are also discussed in this chapter.

By using the derived equation, we discuss the MI when the Kerr media are added in the

PCWs or CROWs in Chapter 3.   In the Chapter 4, the soliton propagation criterion and

pulse broadening at this criterion is discussed.   We found the soliton propagation regions

agree with those of the MI.   In Chapter 5, we investigate the mechanism which causes

the movement of the crossing point of the dispersion relation curves by TBT.   In Chapter

6, the coupling equations of asymmetric PC coupler are derived to discuss mode

switching phenomena and the simulation results by the PWEM.

Chapter 2 Tight binding theory

2.1 Photonic crystal waveguides and coupled resonant optical waveguides

We consider an optical waveguide which consists of a periodic sequence of identical single-mode defects in the PC with lattice constant a_L as shown in Fig. 1. The distance between successive defect points or cavities is a. Assuming the isolated point defect is a single mode with eigenfrequency of ω_0 and electric field distribution in triangular and square lattices as shown in Fig. 2, we can express the electric and magnetic fields of each point defect as $\mathbf{E(r,}t) = \mathbf{E}_0(\mathbf{r})exp(-i\omega_0 t)$ and $\mathbf{H(r,}t) = \mathbf{H}_0(\mathbf{r})exp(-i\omega_0 t)$. Let us assume that the presence of the other defects near a particular site perturbs the total permittivity from $\varepsilon(r)$ to $\varepsilon'(r)$. The fields in the waveguide $\mathbf{E}'(\mathbf{r},t) = \mathbf{E}'_0(\mathbf{r},t)e^{-i\omega_0 t}$ and $\mathbf{H}'(\mathbf{r},t) = \mathbf{H}'_0(\mathbf{r},t)e^{-i\omega_0 t}$ should obey the equations: $\nabla \times \mathbf{E}'_0 = \mu_0(i\omega_0\mathbf{H}'_0 - \partial \mathbf{H}'_0 / \partial t)$ and $\nabla \times \mathbf{H}' = \varepsilon'(i\omega_0\mathbf{E}'_0 - \partial \mathbf{E}'_0 / \partial t)$.

Using the divergence theory of $\nabla \cdot (\mathbf{E}^*_0 \times \mathbf{H}'_0 + \mathbf{E}'_0 \times \mathbf{H}^*_0)$, we can get the Lorentz reciprocity relation [37]:

$$\int d\mathbf{s}(\mathbf{E}^*_0 \times \mathbf{H}'_0 + \mathbf{E}'_0 \times \mathbf{H}^*_0) = \int dv(i\omega_0\Delta\varepsilon\mathbf{E}^*_0 \cdot \mathbf{E}'_0 - \varepsilon'\mathbf{E}^*_0 \cdot \partial\mathbf{E}'_0 / \partial t - \mu_0\mathbf{H}^*_0 \cdot \partial\mathbf{H}'_0 / \partial t) \quad (2.1)$$

with $\Delta\varepsilon=\varepsilon-\varepsilon'$. The electric field $\mathbf{E}'_0(\mathbf{r},t)$ and magnetic field $\mathbf{H}'_0(\mathbf{r},t)$ of the waveguide can be expressed as a superposition of the bound states, i.e., $\mathbf{E}'_0(\mathbf{r},t) = \sum b'_m(t)\mathbf{E}_{0m}$ and $\mathbf{H}'_0(\mathbf{r},t) = \sum b'_m(t)\mathbf{H}_{0m}$, where $\mathbf{E}_{0m} = \mathbf{E}_0(\mathbf{r}-ma)$ and $\mathbf{H}_{0m} = \mathbf{H}_0(\mathbf{r}-ma)$. Substituting these equations into Eq. (1) and letting

$b_m(t) = b_m'(t)e^{-i\omega_0 t}$, we obtain

$$i\frac{db_n}{dt} + (-\omega_0 + P_0)b_n + \sum_m P_m (b_{n+m} + b_{n-m}) = 0. \tag{2.2}$$

Here the coupling coefficient P_m is defined as

$$P_m = \frac{\omega_0 \iiint d\upsilon \Delta\varepsilon E_{0n} \cdot E_{0n+m}}{\iiint d\upsilon (\mu_0 |H_{0n}|^2 + \varepsilon |E_{0n}|^2)}. \tag{2.3}$$

P_0 is a small shift arising from the presence of the neighboring defects. When we consider a plane wave with wave vector k and frequency ω is incident into this waveguide, the dispersion of the waveguide becomes

$$\omega(ka) = \omega_0 - P_0 - 2\sum_{m=1} P_1 \cos(ka). \tag{2.4}$$
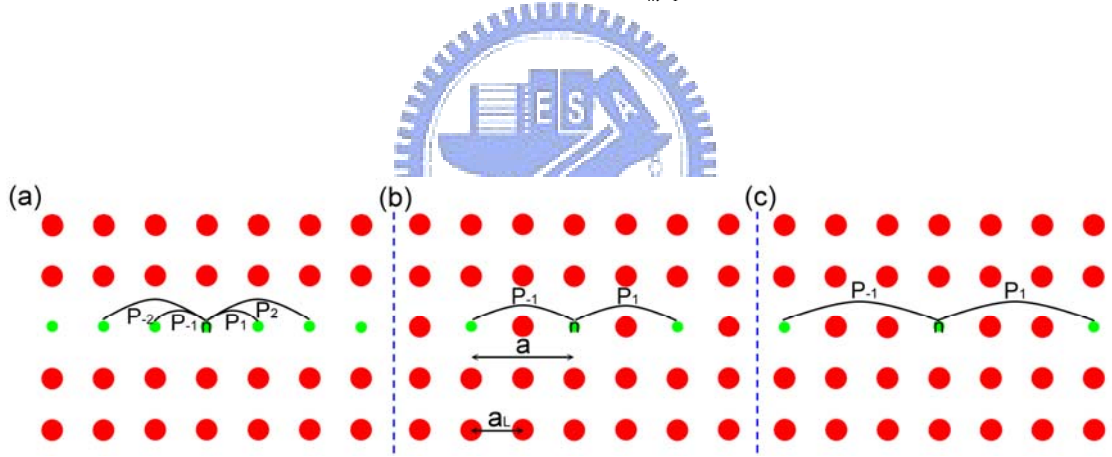
Fig. 1 The structures of (a) a PCW, (b) a CROW with one separation rod and (c) a CROW with two separation rods, where a is the length of successive defect points and a_L is the lattice constant of a PC.
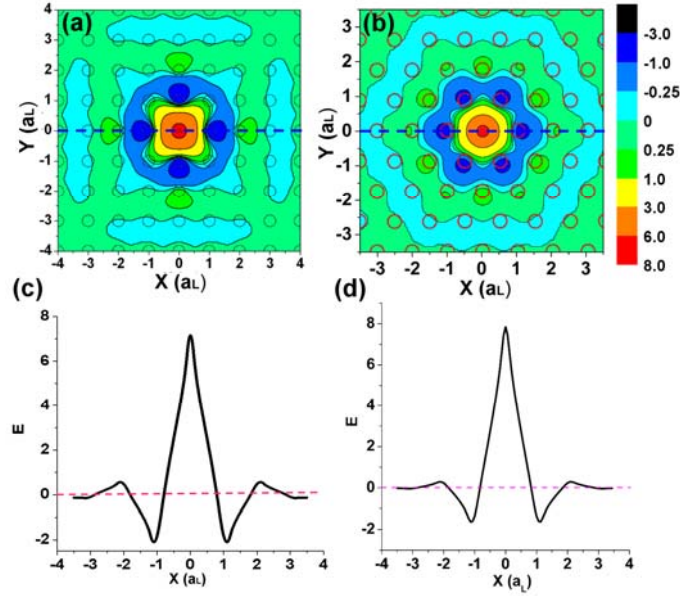
Fig. 2 The electric field distribution (E_z) of a point defect in square lattice for (a) f = 0.364 c/a_L with reduce rod (r_d = 0.05a_L) defect and (b) f = 0.333 c/a with r_d=0.1a_L. (c) (d) The electric field distribution of the blue dash line in (a) (b).

2.2 The properties of coupling coefficients in PCWs and CROWs

The electric field distribution (E_z) of a single point defect, simulated by the PWEM in the square lattice and triangular lattice with the dielectric constant and radii of dielectric rods being 12, 0.2a_L is shown in Fig. 2. The radius (r_d) of the defect rods and eigen frequency in square lattice are 0.05a_L and 0.364 c/a_L; those in triangular lattice are 0.1a_L and 0.333 c/a_L. The field profile along the (blue) dash line in Fig. 2(c) and (d) has the opposite sign when extending to odd nearest-neighbor rod(s) ($\mathbf{E}_0(0,0)*\mathbf{E}_0(xa,0) < 0$, $x =$ 1,3,5,…) and has identical sign when extending to even nearest-neighbor rods [18, 38]. To maintain a single mode propagating in the waveguides, the radius or the refraction index of the rods in the waveguides is reduced therefore $\Delta\varepsilon$ is negative in the following discussion. Since the electric field is mainly localized around the dielectric rods of the waveguides, we can use the maximum values to replace the integral values for a simple

10

estimation of Eq. (2.3).   Therefore, P_1 is positive in even-separated-rod CROWs, in which $\mathbf{E}_0(0,0)^*\mathbf{E}_0(x\mathrm{a},0) < 0$, $x = 1,3$; P_1 is negative in odd-separated-rod CROWs; $|P_2|$ is two orders smaller than $|P_1|$ so P_2 is negligible for considering the dispersion relation. In the PCWs, P_1 and P_3 are positive and P_2 and P_4 are negative; P_3 is two orders of magnitude smaller than P_1, and thus only P_1 and P_2 need to take into consideration when calculating the dispersion relation.   From the dispersion relation in Eq. (2.4), the frequency increases as k increases in PCWs and CROWs with even separation rods where P_1 is positive, but the frequency decreases as k increases in the CROWs with odd separation rods.

2.3 Discrete nonlinear Schrödinger equation

If a Kerr medium ($n^2 = n_0^2 + 2n_0 n_2 |\mathbf{E}|^2$) is added around the defects, Eq. (2.2) can be written as a DNLS equation [37]:

$$i\frac{db_n}{dt} + (-\omega_0 + P_0)b_n + \sum_m P_m(b_{n+m} + b_{n-m}) + \gamma |b_n|^2 b_n = 0. \qquad (2.5)$$

The self phase modulation (SPM) strength is

$$\gamma = \frac{2n_0 n_2 \varepsilon_0 \omega_0 \iiint d\upsilon |E_{0n}|^4}{\iiint d\upsilon(\mu_0 |H_{0n}|^2 + \varepsilon |E_{0n}|^2)} \qquad (2.6)$$

with n_2 being the Kerr coefficient.   Let the plane wave with amplitude ϕ, propagation wave vector k, and frequency ω in site n as $b_n = \phi\,exp(inka\text{-}i\omega t)$ being the solution of Eq. (2.5).   The dispersion relation of the nonlinear PCW can be derived as

$$\omega(ka) = \omega_0 - c_0 - 2c_1\cos(ka) - 2c_2\cos(2ka) - \gamma |\phi|^2 = \omega' - \gamma |\phi|^2 . \qquad (2.7)$$

Here, ω' is the dispersion relation of linear waveguides.   The SPM will make the dispersion relation a constant frequency shift in all wave vectors.   The positive Kerr

coefficient leads a low frequency shift and vice versa.
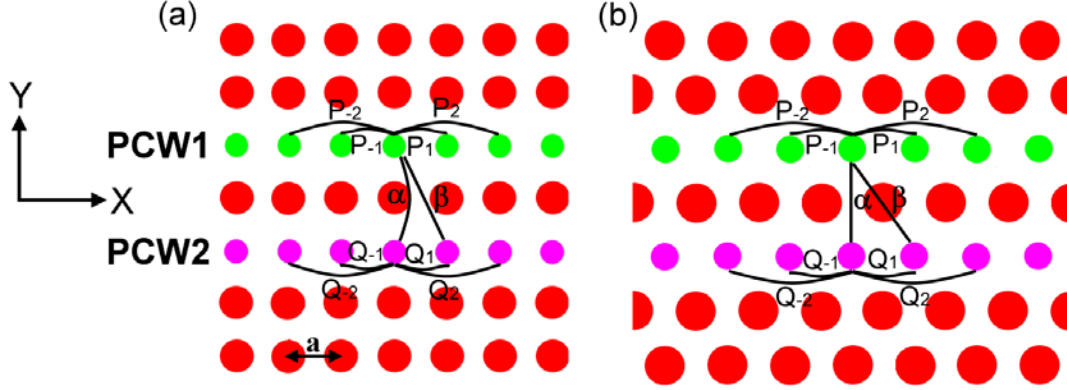
Fig. 3 Geometric structures of the photonic crystal waveguide couplers of (a) square lattice and (b) triangular lattice with the lattice constant a. Ps and Qs are the coupling coefficients between defects within a single waveguide. α, and β are the coupling coefficients between waveguides.

2.4 Coupling equations in asymmetric photonic-crystal coupler

We consider an asymmetric coupled PCWs in a PC with the lattice constant a, in which $a = a_L$, are formed by two rows of periodic defect rods partitioned by a perfect row of rods, shown as PCW1 and PCW2 in Fig. 3 for the square and the triangular lattices, respectively. The field distribution of the eigenmode of an isolated (point) defect in each PCW can be written as the product of time-varying and spatial-varying functions, i.e., $\mathbf{E}_{10}(\mathbf{r},t) = u_0(t)\mathbf{E}_{10}(\mathbf{r})$ in PCW1 and $\mathbf{E}_{20}(\mathbf{r},t) = v_0(t)\mathbf{E}_{20}(\mathbf{r})$ in PCW2, where $u_0(t)=U'\exp(-i\omega_1 t)$ and $v_0(t)= V'\exp(-i\omega_2 t)$, with U' and V' being the constant amplitudes of electric fields and ω_1 and ω_2 the frequencies of localized modes of the point defect in each PCW.

Under the TBT, the evolution equation of the isolated PCW1 can be written as

$$i\frac{\partial}{\partial t}u_n = (\omega_1 - P_0)u_n - \sum_{m=1} P_m(u_{n+m} + u_{n-m}) \qquad (2.8)$$

and $P_m = P_m^{11}$, where P_m^{ij} is the coupling coefficient between the site n of the ith PCW and the site $n+m$ of the jth PCW, and is defined as

$$P_m^{ij} = \frac{\omega_i \int_{-\infty}^{\infty} dv \Delta \varepsilon(\mathbf{r}) \mathbf{E}_{in} \cdot \mathbf{E}_{jn+m}}{\int_{-\infty}^{\infty} dv [\mu_0 |\mathbf{H}_{in}|^2 + \varepsilon |\mathbf{E}_{in}|^2]}. \tag{2.9}$$

Let k and $\bar{\omega}_1$ be the wavevector and its corresponding eigenfrequency of PCW1, respectively, we obtain the dispersion relation of PCW1:

$$\bar{\omega}_1(k) = \omega_1 - P_0 - \sum_{m=1} 2P_m \cos(mka). \tag{2.10}$$

Similarly, the evolution equation and dispersion relation of the isolated PCW2 are shown below:

$$i \frac{\partial}{\partial t} v_n = (\omega_2 - Q_0) v_n - \sum_{m=1} Q_m (v_{n+m} + v_{n-m}), \tag{2.11}$$

$$\bar{\omega}_2(k) = \omega_2 - Q_0 - \sum_{m=1} 2Q_m \cos(mka), \tag{2.12}$$

where $Q_m = C_m^{22}$, $v_n(t)$ and $\bar{\omega}_2$ are the time-varying function and the eigenfrequency of the isolated PCW2, respectively.

Due to the field distributions of defect modes being not strongly localized around defects, we shall consider the coupling effect of two asymmetric PCWs up to the second nearest-neighboring defects, with coupling coefficient $\alpha = C_0^{12} = C_0^{21}$ and $\beta = C_{\pm1}^{12} = C_{\pm1}^{21}$ shown in Fig. 3 for the square and the triangular lattices, respectively. The coupled equations of asymmetric PCWs are given by [39, 40]:

$$i \frac{\partial}{\partial t} u_n = (\omega_1 - P_0) u_n - \sum_{m=1} P_m (u_{n+m} + u_{n-m}) - \alpha v_n - \beta(v_{n+1} + v_{n-1}), \tag{2.13}$$

$$i \frac{\partial}{\partial t} v_n = (\omega_2 - Q_0) v_n - \sum_{m=1} Q_m (v_{n+m} + v_{n-m}) - \alpha u_n - \beta(u_{n+1} + u_{n-1}). \tag{2.14}$$

When the stationary solutions of coupled Eqs. (2.13) and (2.14) are taken as $u_n = U_0$ exp$(ikna-i\omega t)$ and $v_n = V_0$ exp$(ikna-i\omega t)$, we obtain the characteristic equations of the coupler:

$$(\omega - \bar{\omega}_1)\ U_0 + g(ka)\ V_0 = 0, \tag{2.15}$$

$$(\omega - \bar{\omega}_2)\ V_0 + g(ka)\ U_0 = 0, \tag{2.16}$$

where $g(ka) = \alpha + 2\beta Cos(ka)$ and $\begin{bmatrix} U_0 \\ V_0 \end{bmatrix}$ stands for the eigenvector or field amplitudes in

two PCWs. The eigenfrequencies (dispersion relations) and eigenvectors (field amplitudes) of Eqs. (2.15) and (2.16) are

$$\omega^{\pm}(k) = \frac{(\bar{\omega}_1 + \bar{\omega}_2)}{2} \pm \sqrt{\Delta^2 + (g(ka))^2}, \tag{2.17}$$

$$\chi^{\pm} = (V_0/U_0)^{\pm} = -\frac{\Delta \pm \sqrt{\Delta^2 + (g(ka))^2}}{g(ka)}, \tag{2.18}$$

where $\Delta = (\bar{\omega}_2 - \bar{\omega}_1)/2$ and $\chi^{\pm}$ are the amplitude ratios corresponding to frequencies $\omega^{\pm}(k)$. Note that $\chi^{+}\chi^{-} = -1$ is due to the orthogonality of these two eigenmodes at a given wave vector k. At a given frequency, $\chi^{+}\chi^{-}$ is not necessarily equal to -1. In symmetric waveguides, $\bar{\omega}_2 = \bar{\omega}_1$, Eqs. (2.17) and (2.18) will become [41]

$$\omega^{\pm}(k) = \bar{\omega}_1 \pm g(ka), \tag{2.19}$$

$$\chi^{\pm} = (V_0/U_0)^{\pm} = \pm 1. \tag{2.20}$$

The existence of g(ka) makes the eigenstates of the coupler be the linear combination of eigenstates of the single waveguides, leading the EM wave coupled from one waveguide from another. When g = 0, the waveguides will be no longer coupled to each other that means the coupling length is infinite.

In this chapter, we used TBT to derive the coupling equations to describe the electric field propagation in nonlinear or linear single waveguides and linear symmetric or asymmetric PC couplers. In the following chapters, these equations will be used to

further discuss pulse propagation in the PCWs and CROWs with nonlinear media and the

EM wave coupling between two waveguides.

Chapter 3 Modulation instability in a single PCW and CROW

3.1 Introduction

A pulse experiences serious dispersion in the PCWs and CROWs [42, 43]; therefore, it would hardly propagate within the waveguides without broadening.   There are two ideas to improve the situation of allowing the pulse propagation in the waveguides without broadening.   The first method is to design a proper structure to create a linear dispersion curve in the range of operating frequency to provide dispersionless propagation; the other method is to add nonlinear Kerr media to provide soliton propagation [37, 44-46].

However, in the latter case, the criteria of forming a soliton is that the wavevector of the incident wave must be located within the modulation instability (MI) regions [46-48], where the MI refers to a process in which a small perturbation upon a uniform intensity beam would grow exponentially [49].   This phenomenon, which is commonly observed in nonlinear optical fibers [50], will also occur in the nonlinear PCWs and CROWs.

3.2 Modulation instability gain

In Section 2.3, we have derived the DNLS equation to describe the EM wave propagating in PCW or CROWs.   Now, considering a small perturbation $v_n(t)$ superimposed on a plane wave with wave vector and frequency being p and ω, shown as [49]

$$b_n = (\phi + v_n(t))e^{i(pna-\omega t)}, \tag{3.1}$$

we can substitute Eq. (3.1) into Eq. (2.5) in which the 1st and the 2nd nearest-neighbor coupling coefficients are considered to get

$$i\frac{dv_n}{dt}+P_1(v_{n+1}e^{ipa}+v_{n-1}e^{-ipa}-2\cos(pa)v_n)+$$
$$P_2(v_{n+2}e^{ipa}+v_{n-2}e^{-ipa}-2\cos(2pa)v_n)+\gamma|\phi|^2(v_n+v_n^*)=0. \tag{3.2}$$

Taking $v_n(t)$ as this form [49]

$$v_n(t)=(V_1e^{iqna}+V_2^*e^{-iqna})e^{-i\Omega t}, \tag{3.3}$$

where q and ω are the wavevector and frequency of the modulation perturbation, V_1 and V_2^* represent small perturbation with perturbation wavevectors of q and $-$ q, and substituting $v_n(t)$ into Eq. (3.2), we obtained the dispersion relation of the perturbation:

$$\Omega(p,q)=B\pm\sqrt{A(A-\gamma|\phi|^2)} \tag{3.4}$$

with

$$A=4P_1\cos(pa)\sin^2(\frac{qa}{2})+4P_2\cos(2pa)\sin^2(qa) \tag{3.5}$$

and

$$B=2P_1\sin(pa)\cos(qa)+2P_2\sin(2pa)\cos(2qa). \tag{3.6}$$

If the dispersion relation $\Omega(p,q)$ is complex as $A(A-\gamma|\phi|^2)<0$, the perturbation field would become unstable. The intensity growing rate G of MI, also called the MI gain, is related to the imaginary part of $\Omega(p,q)$ by

$$G(p,q)=2*Im(\Omega(p,q))=Re(2\cdot\left|A(\gamma|\phi|^2-A)\right|^{\frac{1}{2}})=2\cdot Re\sqrt{-(A-0.5\gamma|\phi|^2)^2+0.25\gamma^2|\phi|^4}. \tag{3.7}$$

3.3 Gain regions and profiles analysis

Because of $P_2\approx0$ for the CROWs, the coefficient A can be rewritten as $A=4P_1\cos(pa)\sin^2(qa/2)$, in which the sign of A is determined only by pa and it changes sign at $pa=\pi/2$. Here the region of pa (or qa) is defined between 0 and π. For positive (negative) A, γ must also be positive (negative) and $\gamma|\phi|^2>A>0$ ($\gamma|\phi|^2<A<0$) to support

MI, which can be easily derived from Eq. (3.7); in other words, $P_1\cos(pa)\gamma$ must be positive in MI region. Therefore, the boundary of MI must be located at $pa = \pi/2$. In odd-separation-rod CROWs, P_1 is negative, therefore A and γ must be both negative when $0 < pa < \pi/2$ and positive as $pa > \pi/2$. However, in even-separation-rod CROWs, P_1 is positive, therefore A and γ must be both positive when $0 < pa < \pi/2$ and negative as $pa > \pi/2$, shown in Table 1. When the structure of the waveguide (P_1) has been chosen, $|A|$ increases if q increases at constant P_1 and p. When we plot the gain profile as the graph of G vs. q at a given p and define the gain maximum as the maximal values in the graph, from Eq. (3.7), the gain maximum would be located at $A = 0.5\gamma|\phi|^2$ and cut off at $A = \gamma|\phi|^2$ when $4|P_1\cos(pa)| > 0.5|\gamma||\phi|^2$; otherwise, the gain maximum would be located at $qa = \pi$.

Table 1 MI regions of CROWs

Separation rods	Sign of P_1	Sign of $n_2(\gamma)$	MI regions (pa)
Odd	—	+	$> \pi/2$
		—	$< \pi/2$
Even	+	+	$< \pi/2$
		—	$> \pi/2$

In negative (positive) P_1 for an odd-separation-rod (even-separation-rod) case, the slope of dispersion relation is negative (positive) [51] and the frequency dispersion β_2 defined as $d^2\omega/dk^2$ is negative (positive) when $pa < \pi/2$ and positive (negative) for $pa > \pi/2$ from Eq. (2.4). Therefore, for negative β_2 ($pa < \pi/2$ for the odd-separation-rod case and $pa > \pi/2$ for the even-separation-rod case), the negative γ is needed to support MI and positive γ is needed to support MI for positive β_2. In other words, the MI regions of the CROWs in pa can also be decided by simply considering the parameters of β_2 and γ.

In PCWs, P_1 is positive and P_2, which cannot be neglected, is negative. First, we consider the positive Kerr media having positive n_2 (or γ) so the criterion of the MI is $\gamma|\phi|^2 > A > 0$. From the criterion of $A = 4P_1\cos(pa)\sin^2(qa/2) + 4P_2\cos(2pa)\sin^2(qa) > 0$, since P_2 is an order of magnitude smaller than P_1, this criterion can be further reduced to $\cos(pa) > -4|P_2/P_1|\cos^2(qa/2)$. Under this circumstance, the MI region is determined not only by pa but also by qa, and pa in the MI region can exceed $\pi/2$, unlike in CROWs that the MI boundary for pa is located at $\pi/2$ and is independent of qa. From the other criterion: $\gamma|\phi|^2 > A$, we found A is dominated by the P_1 term as pa is located away from $\pi/2$, in this case the MI gain is similar to that in the CROWs with even separation rods. Contrarily, when pa approaches to $\pi/2$, the P_1 term is almost zero and A becomes dominated by the P_2 term. In this case, A would not increase as increasing qa. From Eq. (3.7), we knew that the maximum of the gain profile, G(q), is located at $A = 0.5\gamma|\phi|^2$ or $dA/dq = 0$. For the latter case, the peak gain would be smaller than that of the former condition. When $4P_2\cos(2pa) < 0.5\gamma|\phi|^2$, there would be two gain maxima at a fixed pa and the gain maxima is located at $A = 0.5\gamma|\phi|^2$, but there would be only one gain maximum located at $dA/dq = 0$ as $4P_2\cos(2pa) < 0.5\gamma|\phi|^2$.

On the other hand, in the condition of negative γ, the first criterion is $\cos(pa) < -4|P_2/P_1|\cos^2(qa/2)$. We found the MI would happen only when $pa > \pi/a$. However, when $0 > \cos(pa) > -4|P_2/P_1|$, the MI region is located at the higher q rather than the general case in which the perturbation would have gain at $qa = 0^+$. The cutoff gain is also decided by $A = \gamma|\phi|^2$.

3.4 Simulation results

We consider a square lattice PC with the dielectric constant and radii of the dielectric rods being 12 and $0.2a_L$, where a_L is the lattice constant of the PCs. The radii (r_d) of the defect rods are reduced to be $0.05a_L$ and the Kerr media are introduced around the defects between one separation rod to create the CROW and sequentially to create the PCW. The structures and dispersion relations of the CROW and PCW in TM polarization (the electric field parallels the rod axis) without Kerr media are shown in Fig. 4, which are simulated by the PWEM.
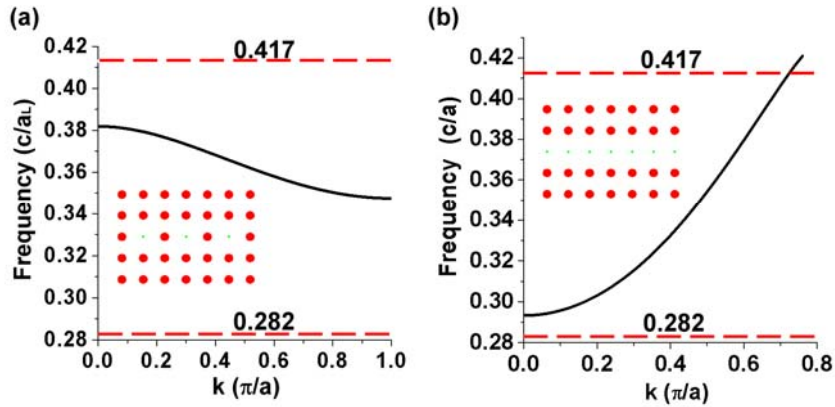
Fig. 4 The dispersion relations of (a) a CROW with one separation rod and (b) a PCW in square lattices, which are simulated by the plane wave expansion method. The dash red lines are the edges of the band gaps.
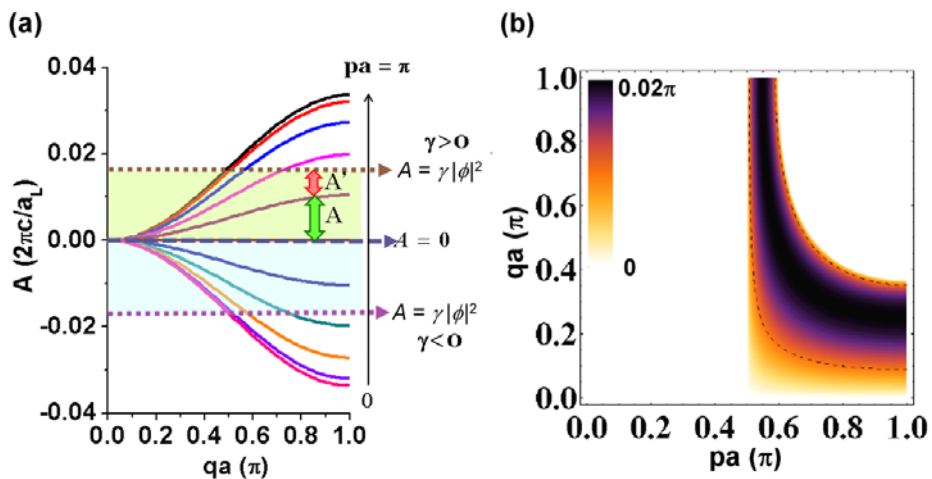
Fig. 5 (a) The values of A and (b) the gains and regions of the MI of the CROW with $\gamma|\phi|^2$=0.01 ($2\pi c/a_L$).

First, the properties of the MI in the CROW would be discussed.   The coupling

coefficient P_1 is -0.00841 ($2\pi c/a_L$), where c is the speed of light in the vacuum.   Because

P_1 is negative, the eigenfrequencies will decrease as increasing k.   Figure 5(a) shows A

vs. qa with different p.   Let $A' = \gamma|\phi_0|^2 - A$ so that $G = 2\sqrt{AA'}$.   As aforementioned, the

MI region is determined by the condition that A lies between 0 and $\gamma|\phi|^2$ and the

maximum of G appears when A equals (or is the closest) to $0.5\gamma|\phi|^2$.   Figure 5(b) shows

$G(p,a)$ with $\gamma|\phi|^2 = 0.01$ ($2\pi c/a_L$).   It can be seen that there is no MI gain when $pa \leq 0.5\pi$

and only a single gain maximum at given pa in the condition of $pa > 0.576\pi$.

In PCWs, the coupling coefficients of P_1 and P_2 are 0.039 and -0.0047($2\pi c/a$), and ω_0-

P_0 is 0.3632 ($2\pi c/a$).   The values of A at a given pa were shown in Fig. 6(a).   When pa

is small, i.e., in [0, 0.4π], A is dominated by P_1 term and A increases as qa increases.

Due to P_1 is positive, the properties of MI would be similar to the CROWs with even

separation rods that possesses a single gain maximum as the solid curve in Fig. 7(a) for pa

= 0.4π.   However, as pa is in (0.4π, 0.6π], A is not simple increasing or decreasing

function of qa, shown in Fig. 6(b).   At a given pa with positive Kerr media ($\gamma > 0$), when

the values of A(q) is always smaller than $0.5\gamma|\phi|^2$, e.g., $\gamma|\phi|^2 = 0.01$ ($2\pi c/a$) and $pa = 0.6\pi$,

there would be a maximal gain as the solid curve in Fig. 7(d).   However, when A(q) is

larger than $0.5\gamma|\phi|^2$, e.g., $\gamma|\phi|^2 = 0.01$ ($2\pi c/a$) and $pa = 0.49\pi$ and 0.55π, there would have 2

gain maxima, solid curves shown in Figs. 7(b) and (c).   And the MI region with positive

γ can extend to $pa = 0.6\pi$, as shown in Fig. 6(c).   On the other hand, the MI region with

negative Kerr media is shown in Fig. 6(d) which is located within $\pi/2 < pa < \pi$ but having

the MI region located at high qa as pa close to $\pi/2$.
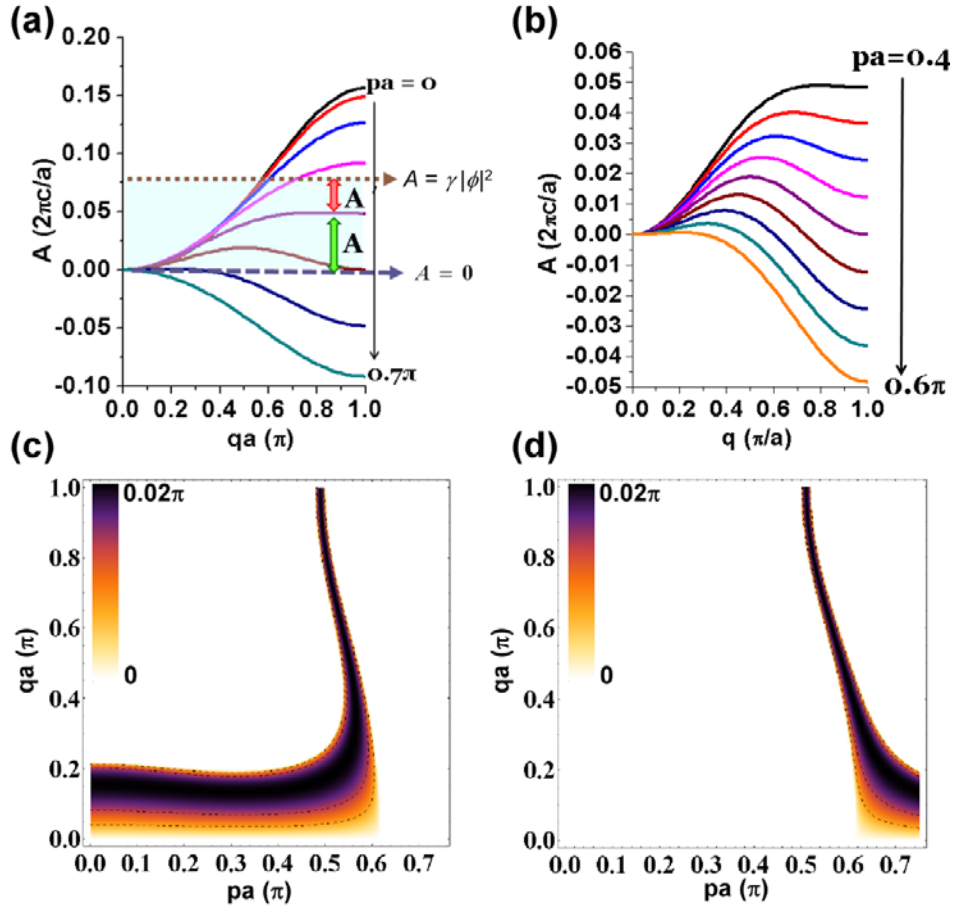
Fig. 6 (a) (b)The values of A in the PCW. The region and gains of MI with (c) positive Kerr media ($\gamma|\phi|^2$=0.01*$2\pi c/a$) and (d) negative Kerr media ($\gamma|\phi|^2$=-0.01*$2\pi c/a$).

Next, we would use the 4th order Runge-Kutta method to simulate the evolution of the perturbation. A plane wave with 10% initial sinusoidal perturbation is used as the input source in a square-array PCW with $\gamma|\phi|^2 = 0.01$ ($2\pi c/a$). The perturbation will grow exponentially in the MI region to become a discrete soliton before it splits, as shown in Fig. 8(a), but the perturbation would never grow outside the MI region Fig. 8(b). We plot the gain coefficients with square dots in Fig. 7 by evaluating the growing rate by the Runge-Kutta method then compare with gain profiles (solid curves) calculated by using Eq. (3.7). The results show a quite good agreement.

22
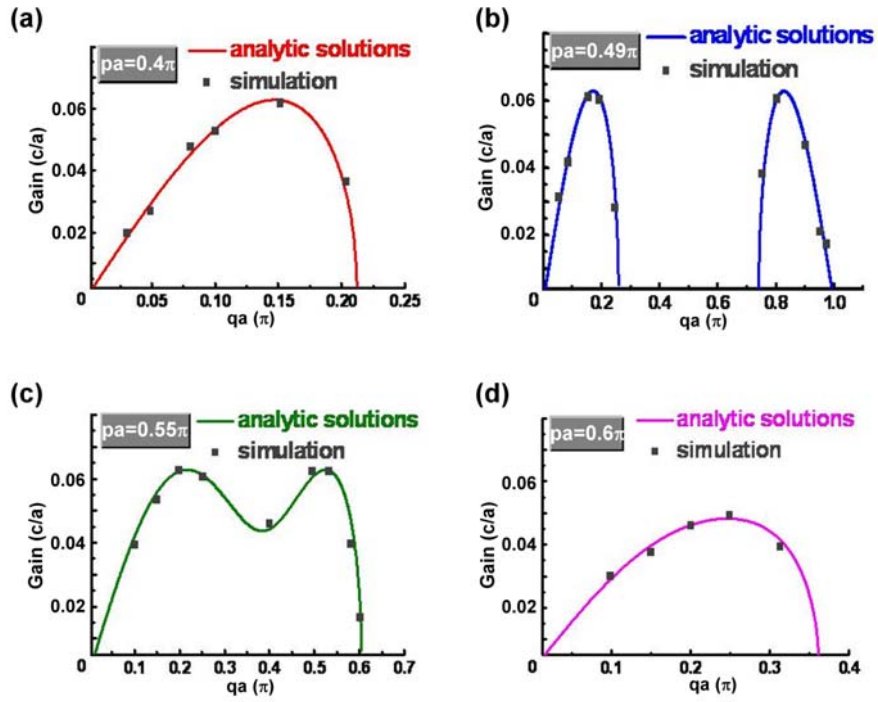
Fig. 7 The MI gain profiles gotten by analytic solution and the simulation by 4th order Runge-Kutta method in different qa with $\gamma|\phi|^2 = 0.01\ (2\pi c/a)$.
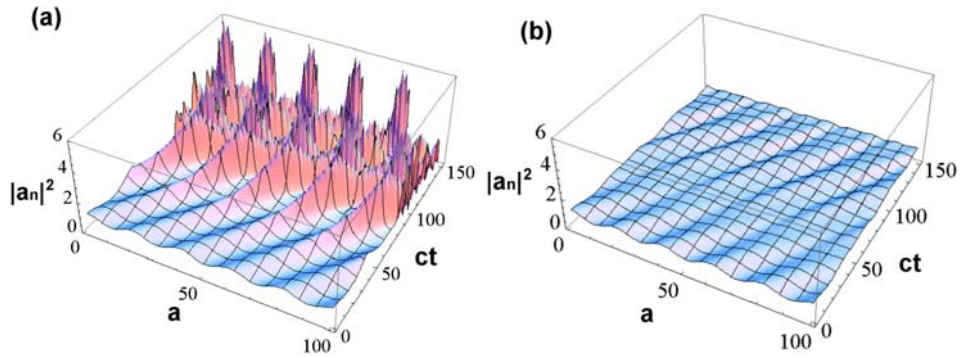
Fig. 8 The evolution of the perturbation in the PCW with (a) pa=0.4π and qa=0.1π (b) pa=0.6π and qa=0.1π.

3.5 Summary

We have successfully used the TBT to investigate the MI in both CROWs and PCWs by considering growth of a small perturbation superimposed on a plane wave.   The

number of separation rods in the CROWs would decide the signs of the nearest-neighbor coupling coefficients (P_1) and the next nearest-neighbor coefficient (P_2) can be neglected because it is more than 2 orders of magnitude smaller than P_1. This leads to positive dispersion for a positive coupling coefficient and vice versa. Although the signs of the coupling coefficient could be different, the criterion: $P_1\cos(pa)\gamma > 0$ for obtaining MI is the same for incident plane wave of wave vector p. Therefore, the MI region can only be located in either $pa < \pi/2$ or $pa > \pi/2$ with only one gain maximum. In the air-defect PCWs, P_1 is positive and P_2, which is no longer negligible, is negative. It makes the MI gain of positive Kerr media located at low wavevectors and vice versus. The boundary of gain region of pa is not exactly at $\pi/2$ due to the MI is mainly dominated by P_2 term as pa approaches $\pi/2$ and there could exist two gain maxima. Furthermore, the numerical simulation using the 4th order Runge-Kutta method reveals exponentially growing perturbation intensity as it propagates and the growing rate matches with the gain coefficient of MI in the analytic solution.

In next chapter, a pulse will be incident into the waveguide within or without the MI region to understand if a soliton can exist in the MI region. At the same time, the soliton propagation criterion will also be derived to observe the soliton propagation under this criterion.

Chapter 4 Soliton propagation in a single PCW and CROW

The amplitude evolution of the electric field in the nonlinear CROWs containing Kerr media often leads to DNLS equation derived by the TBT [37, 51-53] and Section 2-3. By solving the DNLS equation under long-wavelength approximation, this equation reduces to a nonlinear Schrödinger (NLS) equation. Spatiotemporal discrete solitons can propagate undistorted along the defects by balancing the effects of discrete lattice dispersion with material nonlinearity [37]. However, as the pulse becomes narrow, the long-wavelength approximation will be broken and high order dispersions should be considered [53]. Therefore, the more generalized criteria for solitons propagation in different structures of CROWs [51], e.g., different numbers of separation rods between two cavities or different pulse widths, should be derived. Moreover, in the PCWs, the defect rods are so close that the next nearest-neighbor coupling cannot be neglected [41]. The governed equation of motion is termed the extended discrete nonlinear Schrödinger (EDNLS) equation to distinguish the equations in CROWs in which only the nearest-neighbor coupling coefficient is considered. There are rare reports on pulse propagation in nonlinear PCWs using the TBT but the Green-function approach[44, 45]. Although the equations obtained from these two approaches are quite similar [54], it still lacks on the research about the dynamic or criteria of soliton propagation in the PCWs. Therefore, it is needed to take the advanced discussion about criteria of solitons propagation of different kinds of CROWs or PCWs, and to derive the EDNLS evolution equation for describing the dynamic properties of solitons with different nonlinear strengths and pulse widths.

4.1 Soliton propagation criteria

In order to get the soliton solution and to give the advanced analysis of high-order dispersion as pulse propagating, we let $x = na$ and $b_n = \phi e^{i(kx-\omega't)}$. Taking the Taylor' expansion of ϕ [53]

$$\phi(x+a) = \phi + \sum_{n=1} \frac{a^n}{n!} \frac{\partial^n \phi}{\partial x^n}, \tag{4.1}$$

Eq. (2.5) can be written as a NLS equation:

$$i \frac{\partial \phi}{\partial t} - \sum_{n=1} \frac{(-i)^n}{n!} \beta_n \frac{\partial^n \phi}{\partial x^n} + \gamma |\phi|^2 \phi = 0. \tag{4.2}$$

The dispersion coefficients, β_n, equal to $\partial^n \omega(k)/\partial k^n$ or

$$\beta_{2n-1} = 2a^{2n-1}(-1)^{n+1} \sum_{m=1} m^{2n-1} P_m \sin(mka), \tag{4.3}$$

$$\beta_{2n} = 2a^{2n}(-1)^{n+1} \sum_{m=1} m^{2n} P_m \cos(mka). \tag{4.4}$$

Therefore, the angular frequency of the waveguides can also be expressed as the Taylor' expansion sum of dispersion coefficients, i.e.,

$$\omega(k) = \omega_0 + \beta_1 \Delta k + \beta_2 (\Delta k)^2 / 2! + \beta_3 (\Delta k)^3 / 3! + \cdots, \tag{4.5}$$

where β_1 is the group velocity (v_g) of the solitons in these waveguides if the high-order terms is neglected. When the variation of the pulse amplitude is smooth enough, i.e., $\beta_n (\Delta k)^n / n! \approx 0$ or $\beta_n \frac{\partial^n \phi}{\partial x^n} \approx 0$ for $n > 2$, Eq. (4.2) has a soliton solution as

$$b = \phi \operatorname{sech}(\frac{x - \beta_1 t}{x_0}) e^{i(kx-\omega t)}. \tag{4.6}$$

The criterion to support a soliton propagation is thus $\gamma \phi_0^2 = \beta_2 / x_0^2$ or

$$\gamma \phi^2 = 2a^2 (P_1 \cos(ka) + 4P_2 \cos(2ka) + 9P_3 \cos(3ka) + \cdots)/x_0^2. \tag{4.7}$$

From Eq. (4.6), the dispersion relation of the soliton is the same as a plane wave incident

into the nonlinear waveguides.   The relationship between x_0 and ϕ_0 is determined by β_2 and γ (n_2 or $\chi^{(3)}$).   The sign of β_2 and γ must be the same to support a soliton propagation and SPM strength (γ_s) is $\beta_2 / (x_0^2 \phi^2)$.

In the CROWs, P_2 is two orders of magnitude smaller than P_1, so P_2 can be neglected in considering β_2 and the soliton propagation criterion (SPC) in Eq. (4.7) can be further reduced to $x_0^2 / a^2 = 2P_1 \cos(ka) / (\gamma \phi^2)$.   In even separated rods, P_1 is positive so γ should be positive at the SPC when $ka < \pi/2$ and γ should be negative as $ka > \pi/2$; however, in odd separated rod(s), P_1 is negative so γ should be negative (positive) at the SPC when $ka < \pi/2$ ($ka > \pi/2$), which correspond to the MI in these nonlinear waveguides [38] and the Kerr media should switch their signs when ka crosses $\pi/2$.   In PCWs, P_1 is positive and P_2 is negative with its value being an order of magnitude smaller than P_1 [23]. Therefore, positive Kerr media should be put in the waveguides as a low wave vector or low frequency EM wave is incident, and vice versa.   When the coupling coefficients P_n ($n > 2$) are neglected for a simply estimation, Eq. (4.7) can be written as $\cos(ka) = -4 \mid P_2/ P_1 \mid$ if $\gamma = 0$.   Therefore, the border of switching sign of Kerr medium for soliton propagation in PCWs occurs at $ka > \pi/2$.   However, if the dielectric defect is used, in which $\Delta\varepsilon > 0$, the signs of P's should be changed and the type of Kerr media would also be changed accordingly.

4.2 Pulse broadening due to the high-order effect

To estimate the influence of high-order dispersion which makes the pulse broadening, and the width of the soliton pulse that can make the high-order term negligible, we took

the Fourier transform of the soliton solution, sech(x/x_0), and calculated the standard deviation of k's distribution as $\Delta k = 1/x_0$.   Taking derivative of Eq. (4.5) with respect to k, the group velocity can be expressed as

$$\partial\omega / \partial k = \beta_1 + \beta_2(\Delta k) + \beta_3(\Delta k)^2 / 2! + \beta_4(\Delta k)^3 / 3! + \cdots. \tag{4.8}$$

When the dispersion of β_2 is balanced by the SPM and $x_0 > a$, the pulse broaden will mainly dominated by the lowest nonzero dispersion coefficients, β_n, having $n > 2$.   As the GVD arises from β_3 is determined by $0.5\beta_3\Delta k^2$ and is proportional to $(1/x_0)^2$.   The dispersion can be neglected when $0.5\beta_3\Delta k^2 t \approx 0$.   At a particular frequency in which $\beta_3 = 0$, Eq. (4.5) can be rewritten as

$$\omega = \omega_0 + \beta_1\Delta k + \beta_2(\Delta k)^2 / 2!(1 + (\beta_4 / \beta_2)\Delta k^2 / 6)) + \cdots. \tag{4.9}$$

From the dispersion relation in Eq. (2.7), the signs of β_2 and β_4 are opposite in all propagation frequency of the CROWs and in mostly propagation frequency of the PCWs. Therefore, the term of $(1 + \beta_4 / \beta_2 \Delta k^2 / 6)$ will be smaller than or equal to 1.   We should reduce the SPM strength (γ_s) to prevent overall SPM strength from making the pulse narrowing, especially when the pulse width is short for large β_4 and small (or zero) β_3 at ka approaches 0 or π.   However, when the pulse is seriously dispersed in the waveguide, it is no longer having the form of hyperbolic secant (HS), the dispersion would be dominated by the β_2 term again.

4.3 Simulation results and discussion

We consider triangular-lattice PCs with the dielectric constant and radius of the dielectric rods being 12 and $0.2a_L$.   The radius (r_d) of the defect rods is reduced to $0.1a_L$ and the Kerr media are introduced in the defects between one separation rod to create the

CROW and sequentially to create the PCW as shown in Figs. 9(a) and (b). The dispersion curves, which were simulated by the PWEM, and dispersion coefficients (β_n) of the CROW and PCW in TM polarization without Kerr media are shown in Figs. 9(c) and (d). The coupling coefficient of P_1 is -0.00652 ($2\pi c/a$) in the CROWs and P_1, P_2 and P_3 are 0.02041, -0.00205 and 0.00026 ($2\pi c/a$) in the PCWs.
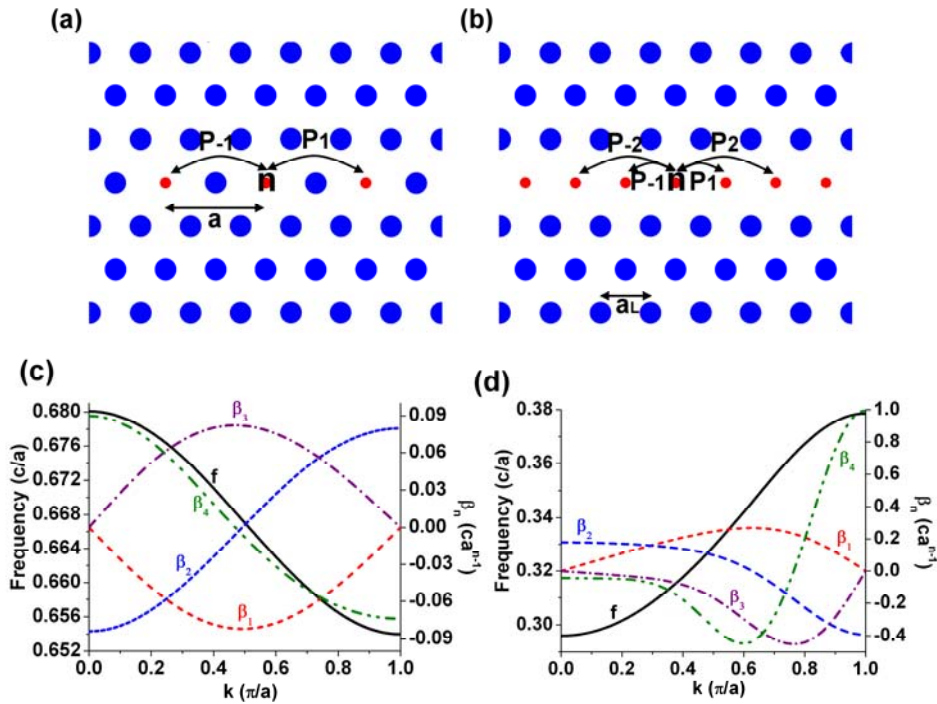
Fig. 9 (a) The structure of a CROW with a separation rod and (b) of a PCW in triangular lattice. The dispersion relations and dispersion coefficients of (c) a CROW with one separation rod and (d) a PCW in triangular lattices calculated by the plane wave expansion method.

Due to the magnitude of the coupling coefficients in the CROW is smaller than those in the PCW, the magnitude of the group velocity (β_1) and the higher dispersion coefficients ($\beta_{2,3,4}$) in CROWs would be smaller than in PCWs. However, because the signs of P_1's are different so that the EM waves in these two structures will propagate in the opposite directions. The neglected P_2 term in CROWs makes $\beta_2 \approx 0$ and the values

of β_3 is almost symmetric at $ka = \pi/2$, leading to soliton propagations at k and $1-k$ (in π/a unit) would be similar if different signs of Kerr media were introduced in the defects. However, it would behave quite differently in the PCWs.   The border of switching sign of Kerr medium for soliton propagation occurs at $ka > \pi/2$, and the high-order dispersion coefficients (β_3, β_4) in high k is larger than those in low k due to the negligible 2nd and 3rd next-neighbor coupling coefficients.

We will use the 4th order Runge-Kutta method to solve Eq. (2.5) to simulate an initial HS pulse propagating in the PCW and CROWs, because the HS pulse is a soliton solution. The advantage of using this method is to directly solve Eq. (2.5) without the requirement of calculating the dispersion coefficients.   However, when the split-step Fourier method [53, 55] is used to solve Eq. (4.2), all orders of the dispersion coefficients are required to take into consideration for short pulse.   On the other hand, if a Gaussian pulse is incident into the nonlinear waveguides with the same energy of the HS pulse at the SPC with small high-order GVD, the Gaussian pulse will initially develop into HS envelope, then finally the pulse becomes broadened due to the high-order dispersions that behaves like initially launching the HS pulse into the nonlinear waveguides.

4.3.1 Soliton propagation in the coupled resonant optical waveguides

To observe the pulse broadening without Kerr media or under the SPC, where $\gamma_s = 2c_1 a^2 \cos(ka)/(\phi^2 x_0^2)$ in the CROWs with one separation rod and γ_s (n_2) is positive as $ka > \pi/2$, we sent a hyperbolic-secant (HS) wave, i.e., $\phi \operatorname{sech}(x/x_0)e^{ikx}$ with $x_0 = 2a$ into the CROWs and let it propagate $400a/c$ in different k's as shown in Fig. 10.   It can be seen that the pulse would spread seriously without Kerr medium but spread slightly or

even preserve at the SPC. Because $\beta_2 = 0$ at $ka = 0.5\pi$, the pulse would not spread even without Kerr medium, whereas, the dispersive waves were observed at the farther distance wing with the larger x in Fig. 10(a) due to the higher order dispersion β_n with n > 2. From Fig. 9(a) we noticed that β_2 monotonically increases, without Kerr medium the pulse becomes broader as increasing k as shown in Fig. 10(a) and it is the broadest at $ka = \pi$. At the SPC, however, β_2 can be balanced by the SPM and thus the pulse is basically preserving the same shape without broadening except for the larger β_3 as ka approaches 0.5 π. Because $\beta_3 = 0$ at $ka = 0$ or π, it makes soliton propagation almost with no dispersive waves and the pulse disperse symmetrically in the waveguides even containing no Kerr media.
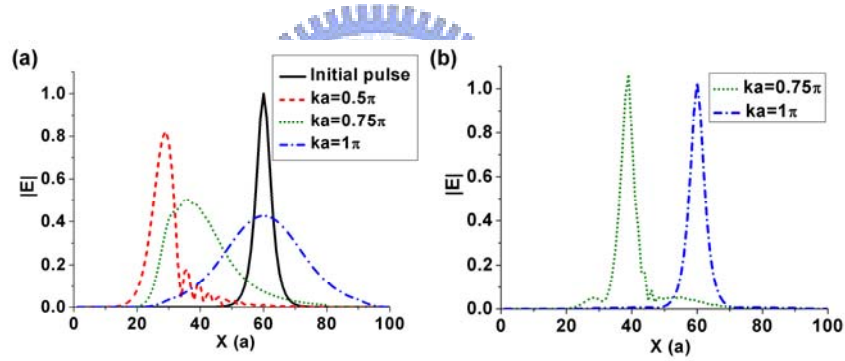
Fig. 10 The hyperbolic-secant (HS) pulse ($x_0 = 2a$) propagates in the CROWs of different wave vectors at $t = 400a/c$ (a) without Kerr medium and (b) at the soliton propagation criterion by using the 4th order Runge-Kutta method.   The black solid line in (a) is the incident pulse.

4.3.2 Soliton propagation in the photonic crystal waveguides

In the PCWs, in order to further evaluate the degree of the pulse broadening arising from high-order dispersions, we define the broadening factor (BF) as σ/σ_0, where σ is the root-mean-square energy of output pulse and σ_0 is that of the input pulse.   From the BF of PCWs at different propagating time (T) for $ka = 0.6\pi$ and 0.75π as shown in Fig. 11 (a), the BF is proportional to $1+T^2$ as the BF is small, but it is proportional to $1+T$ when BF

>> 1, which corresponds to the Gaussian pulse propagating in the PCWs [55]. The BF ($ka = 0.75\pi$) > BF (0.6π) initially, but becoming reversely with BF (0.6π) > BF (0.75π) after the pulse propagates a span of 60 a/c for $x_0 = 2a$. This is because the BF is mainly dominated by β_3 at the SPC but dominated by β_2 after having been severely distorted by β_3. However, when $ka = 0.9\pi$ and $x_0 = 2a$, the BF would become smaller, which means that the pulse width becomes narrower and its peak electric field becomes higher. It is due to the opposite signs of β_2 and β_4 make SPM at $\gamma = \gamma_s$ too strong, especially when β_4 is much larger than β_2 and $\beta_3 = 0$ with small x_0. At $\gamma = 0.9\gamma_s$, the pulse width would become less broadening and neither further narrowing as time passes as shown in Fig. 11(b). Once the pulse width becomes wider, the high-order dispersions become negligible. The overall self phase modulation at $\gamma = \gamma_s$ should not be apparent.
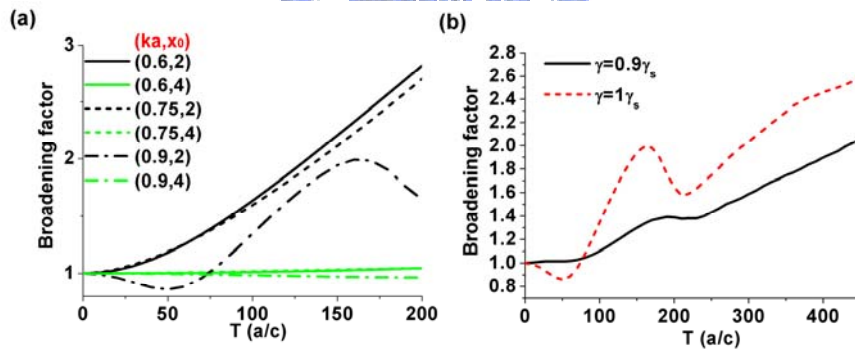
Fig. 11(a) The broadening factor of $ka = 0.6\pi$, 0.75π, and 0.9π and $x_0 = 2a$ and $4a$ of the HS envelope at the SPC and (b) the broadening factor of $\gamma = 0.9\gamma_s$ and $1\gamma_s$ at $ka = 0.9\pi$ and $x_0 = 2a$.

The broadening mechanism and the formula to define the SPCs in CROWs and PCWs are similar but the condition (γ or k) to support the SPC is quite different due to the difference of the coupling coefficients. Once when the coupling coefficients are obtained by the PWEM, the pulse broadening and the SPC can be well analyzed by the

derived equations.   The simulation results obtained from the 4th order Runge-Kutta method agree well with our analyses in both the CROWs and PCWs.

4.4 Summary

The soliton propagation in the CROWs and the PCWs containing optical Kerr media was studied using the tight-binding theory.   By considering the coupling between the defects, we derived an extended discrete nonlinear Schrödinger equation to describe the wave propagation in these nonlinear waveguides.   By solving this equation, we obtained the criterion which supports the soliton propagation if the dispersion more than three orders can be neglected or the dispersion can be highly depressed at the criterion if the high order dispersions cannot be neglected.   In CROWs, the different kinds of Kerr media (positive or negative Kerr coefficients) should be added if the wave vector of the propagation wave (before or after $\pi/2a$) or separated rods (odd or even) are different but the signs of the second order dispersion coefficients of the waveguides and three-order susceptibility of the Kerr media must be identical. Due to the coupling coefficients in the PCW are larger than that in the CROW, the group velocity and the dispersion should also be larger in the PCWs, making SPM stronger to support solitons propagation in the PCWs. When the pulse width is long enough, only the first nonzero β_n with n> 2 should be taken into consideration for pulse broadening but as the pulse width becomes shorter, the high-order dispersions become more significant to make the SPM smaller than the criteria when β_3 approaches zero.

In Chapters 3 and 4, we have discussed the pulse propagation in the single PCW and CROW.   In the next chapter, another identical waveguide will be carved into the PC with one or several partition rods to investigate the wave coupling between two waveguides.

Chapter 5 Tuning the decoupling point of a photonic-crystal directional coupler

There are two dispersion curves with one even mode and one odd mode in a symmetric directional coupler (DC). The field amplitude of EM wave propagating along the DC can be expressed as the linear combination of these eigenmodes and the coupling length of a DC is defined as $\pi/\Delta k$, where Δk is the wave vector mismatch of these eigenmodes [41]. In a triangular lattice PCs made of dielectric rods in the air, the dispersion curves of a DC will cross at a particular wave vector. At this crossing point, named as the decoupling point, the coupling length becomes infinite so that the EM wave incident from one PCW will never be coupled into the other PCW. In a square lattice of PCs, however, only the DC made of removed rods or reduced rods with small radii of dielectric will make dispersion curves crossed at the wave vector near the Brilluoin-zone boundary. Using the infinite coupling length for one wavelength and a finite coupling length for another, we have designed a miniature bidirectional coupler [30, 31], in which knowing the crossing point and coupling length in advance is an important issue. Here, we propose using the TBT to control these two parameters and derive the design rules for DC [56].

5.1 Theory analysis

We consider a TM-polarization wave propagating in a PCW, which consists of one row of reduced rods in a square (triangular) lattice of dielectric rods in air with lattice constant

a, shown in Fig. 12(a).   By applying TBT to these cases which is derived in Section 2.1, we can express the amplitude (u_n) of the electric field in the site n as [57]

$$i\frac{\partial}{\partial t}u_n = (\bar{\omega}_1 - P_0)u_n - \sum_{m=1} P_m(u_{n+m} + u_{n-m}),$$ (5.1)

where $\bar{\omega}_1$ is the eigenfrequency of a single point defect, P_0 represents a small shift to the eigenfrequency $\bar{\omega}_1$ due to the dielectric perturbation of the neighboring defects to the point defect at site n, and P_m is the coupling coefficient between sites *n* and *n+m*. The dispersion relation of a single PCW can be written as

$$\omega_1(k) = \bar{\omega}_1 - P_0 - \sum_{m=1} 2P_m \cos(mka).$$ (5.2)

Here, P_0 causes the relative frequency shift for all wave vector k from $\bar{\omega}_1$, whereas P_m's cause the sinusoidal modulation.
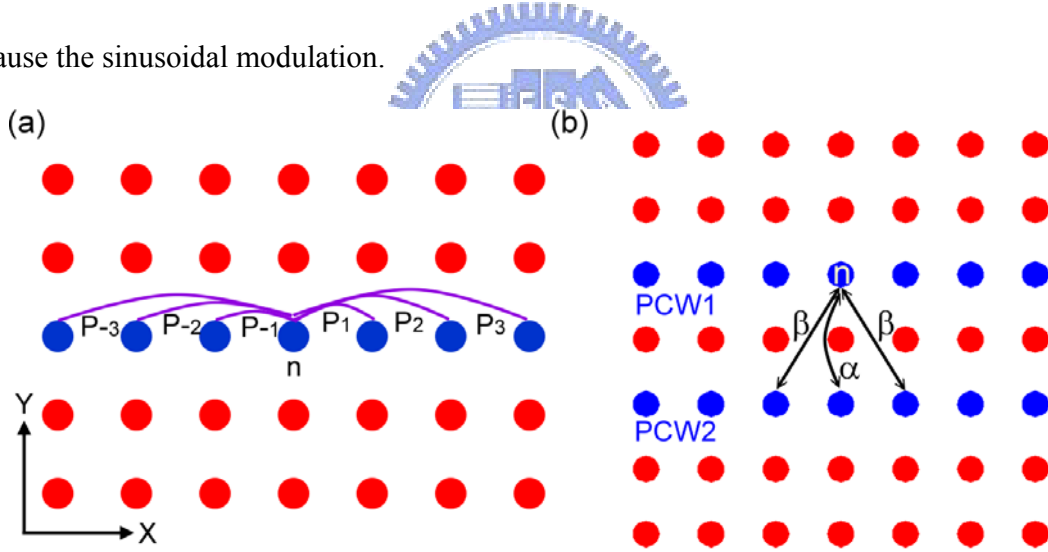

Fig. 12 Geometric structures of (a) single and (b) double PCWs with the lattice constant *a*. P_m's are the coupling coefficients between defects within a single waveguide. α and β are the coupling coefficients between waveguides.

5.1.1 Eigen frequency shift and dispersion relation shifts of moving point defects in PCWs

Moving the point defect along ±y (or ±x) direction in the square lattice will shift the eigenfrequency ($\bar{\omega}_1$) of a point defect toward the higher frequency as shown in Fig. 13(a). Such a blue shift in frequency is caused by less concentration of electric fields in the dielectric defect rod [58] when the defect rod moves away from the center as shown in Fig. 13(b) for field distribution along the y-direction and Fig. 13(c) for that along the x-direction. From Fig. 13(c) the field distribution is almost unchanged along the propagation axis (the x-direction) of PCW so that it would remain unaffected. Therefore, the dispersion curve should just show a blue shift after moving all the defect rods along y direction in the PCW (see Fig. 14(a)). However, if moving all the defect rods of the PCW along the x-direction, shown in Fig. 14 (b), one would increase both $\bar{\omega}_1$ and P_0 but only slightly change P_m's. Therefore, we would expect that the dispersion curve is almost unchanged at small wave vector k and slightly increases at the larger wave vector k by translating all the defects along the x-direction.
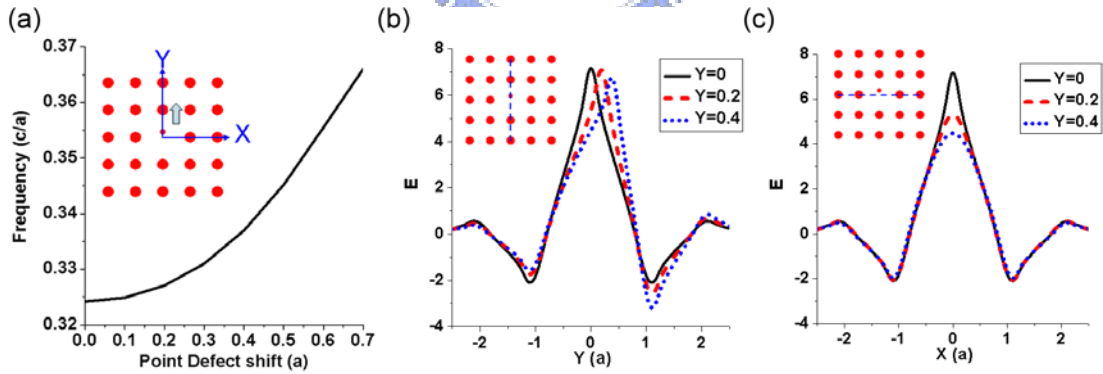
Fig. 13 (a) The eigenfrequencies, (b) the electric field along the y axis, and (c) the electric field along the x axis of the point-defect modes with a defect rod located at different positions along the y axis, where c is the speed of light in vacuum.
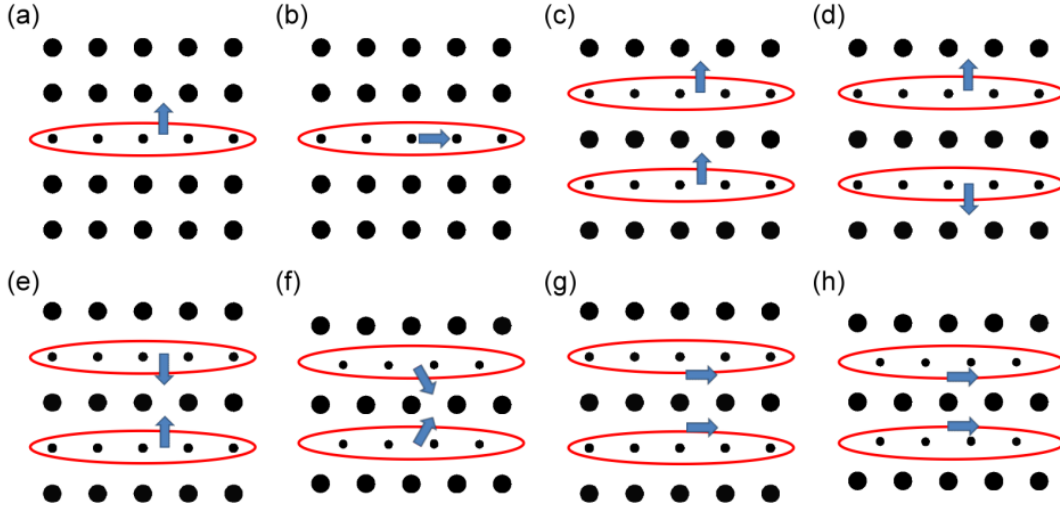
Fig. 14 The ways of moving the defect rods in single or coupled PCWs.

5.1.2 Dispersion relation shifts in photonic-crystal couplers

When a second identical waveguide is created to make a symmetric DC, shown in Fig. 12(b), the amplitudes of electric fields (U_0, V_0) in PCW1 and PCW2 are given by the coupled equations:

$$(\omega - \omega_1)U_0 + (\alpha + \beta Cos(ka))V_0 = 0, \qquad (5.3)$$

$$(\omega - \omega_1)V_0 + (\alpha + \beta Cos(ka))U_0 = 0, \qquad (5.4)$$

where α and β are the coupling coefficients of one PCW induced by the nearest-neighbor and the next-nearest neighbor defect rods of the other PCW; ω_1 and ω are the eigenfrequencies of the single PCW and the DC, respectively. Solving for Eqs. (5.3) and (5.4), we obtained the dispersion relations of the DC:

$$\omega(k) = \omega_1(k) \pm (\alpha + 2\beta \cos(ka)), \qquad (5.5)$$

where the plus sign stands for the odd mode and the minus sign for the even mode [24]. The dispersion relations of the DC split from $\omega_1(k)$ with their frequency difference being determined by coefficients α and β. Whether the dispersion curves cross at a point or

not is determined by the ratio $\zeta=|2\beta/\alpha|$ [57]. As the PCWs are formed by moving all the

defect rods along the y-direction, shown in Fig. 14(c), we would expect that there exists a

larger ω_1 and barely changes in α and β because the distance of the defect rods between

two waveguides is unchanged. Therefore, the dispersion curves of the DC would show

only a blue shift. As enlarging the distance between two line defects in the DC by

oppositely moving all the defect rods along the y direction as shown in Fig. 14(d), we

would expect that coefficients α and β become smaller and there is a reduced coupling of

PCWs. Thus it would reduce the frequency separation between two dispersion curves,

which shift together toward the higher frequency. On the other hand, as reducing the

separation of the line defects, shown in Fig. 14(e), we can increase the separation of the

dispersion curves, which both shift to the higher frequency. In addition, similar effects

showing in a square lattice are reproduced by reducing the separation of the line defects of

DC in a triangular lattice, shown in Fig. 14(f).

   Moving all the defect rods along the x axis, shown in Figs. 14(g) and (h), will change

the ratios of electric fields at (0,2a) and ($\pm$1a, 2a) in the square lattice so that the

coefficients α and β would also change. It makes the decoupling point moved to

different wave vector k. The larger ζ makes the decoupling point moved to the smaller

wave vector k. Let the ratio ζ and the electric field before (after) moving all the defect

rods along the x-axis as ζ_1 (ζ_2) and E_1 (E_2), respectively. Assuming the field distribution

is strongly localized at the dielectric rods, we can simply use the ratio of the maximal

field values instead of integrals as Eq. (2.9) to estimate coefficients α, β and ζ. Thus,

$$\zeta_2/\zeta_1 \approx (E_2(-a,2a)/E_2(0,2a))/(E_1(-a,2a)/E_1(0,2a)). \qquad (5.6)$$

From the field distribution before and after shifting the defect rods shown as in Fig. 15,

we obtained $\zeta_2/\zeta_1 > 1$ in square lattice but $\zeta_2/\zeta_1 < 1$ in triangular lattice. Therefore,

moving all defects along the x-direction in the square lattice will create dispersions'
crossing and further shift toward the smaller wave vector k with increasing the moving
distance in the x-direction. However, in the triangular lattice, the decoupling point
shifted toward the larger wave vector k. These phenomena are due to the lattice
structure of the former case being getting close to a triangular one which possesses
dispersions' crossing on translating the line defects along the x-direction; while that of
latter case tends to become a rectangular one.
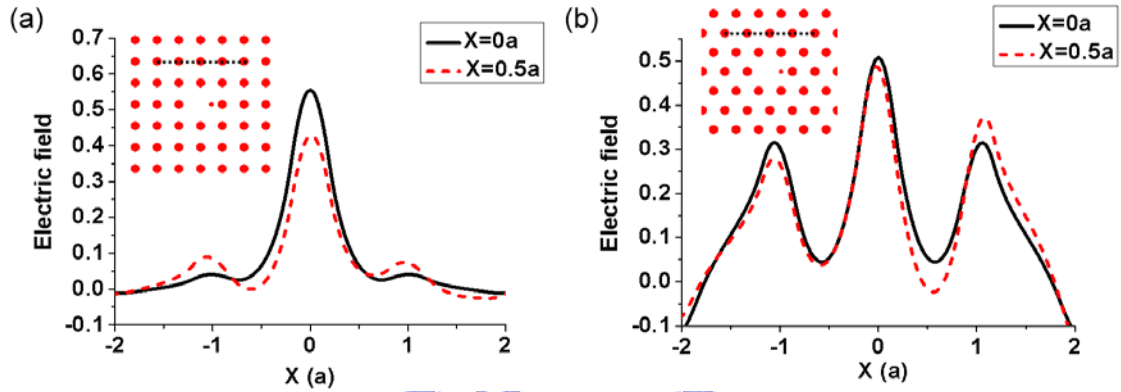
Fig. 15 The electric field distribution of the point defect mode before (x = 0a) and after moving
the defect rods by 0.5a along the x-axis (x=0.5a). (a) The electric field located at y = 2a in the
square lattice and (b) the electric field located y = $\sqrt{3}a$ in the triangular lattice.

5.2 Simulation results and discussion

In the previous section, we have used the TBT to analyze the variation of dispersion
curves by moving defects in the DCs that causes the change of eigenfrequency of a single
PCW and coupling coefficients P_m, α and β. Here, we will use the PWEM and the
FDTD to examine the proposed design rule for a PC with the radii and the dielectric
constant of the dielectric rods being 0.2a and 12, respectively. The radii of the defect
rods in the square lattice are 0.1a and 0.09a in the triangular lattice.

Firstly, we examined a single PCW with all line defect rods being transversely moved (along the y-axis) in the square lattice using the PWEM. We can see that the dispersion curve in Fig. 16(a) shifts completely to the higher frequency, which means that the coupling coefficients P_m between defect rods are unaffected during transversely moving all defect rods. The frequency shift is mainly dominated by the variation of the eigenfrequency ($\bar{\omega}_1$) of the point defect as moving the defect rod. However, as the defect rods moved along the x-axis shown in Fig. 16 (b), both $\bar{\omega}_1$ and P_0 would increase and cancel out the effect of changing eigenfrequency ω_1 in the regime of small wave vectors, whereas the dispersion curve bends down in the regime of large wave vectors, due to the high-order terms $P_m\cos(mka)$ becoming important.
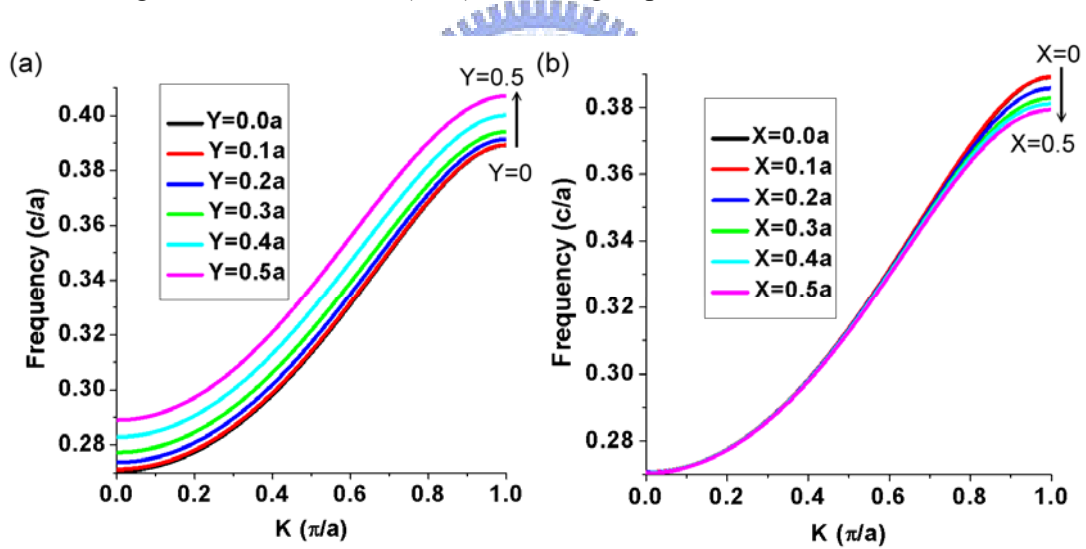

Fig. 16 Dispersion curves of a single PCW with all the defect rods moving along (a) the y-direction, and (b) along the x-direction.

Secondly, by transversely moving defect rods separately, Figure 17 shows how the dispersion curve varies as changing the structure of the DC. Here, we used the square lattice as a demonstration because there are similar results in square lattice and triangular

lattice. As simultaneously moving two line defects off the center of the original PCWs and keeping the separation between PCWs fixed, we find the dispersion curves shift toward the higher frequency as shown in Fig. 17(a). On the other hand, the reduction of the separation of the line defects to decrease the coupling between PCWs pushes the dispersion curves apart (see Fig. 17(b)); whereas, symmetrically enlarging the separation of the line defects not only shifts the dispersion curves toward high frequencies but also makes two dispersion curves closer (see Fig. 17(c)).
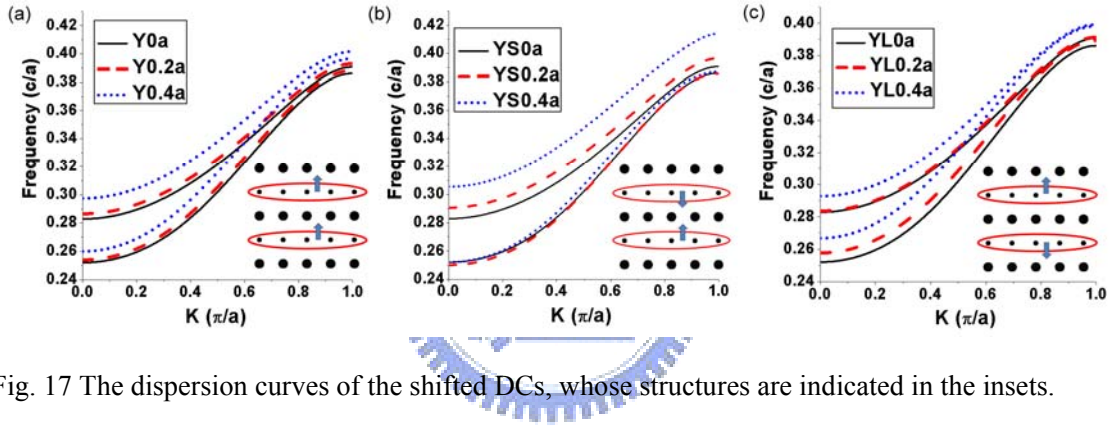
Fig. 17 The dispersion curves of the shifted DCs, whose structures are indicated in the insets.

Thirdly, we examined the effects of moving all the defect rods along the x-direction in Fig. 18. We found that the dispersion relations, originally showing no decoupling point, in a square lattice become cross at a high frequency as the symmetry is broken. And the decoupling point moves toward the lower frequency or the smaller wave vector k as the rods are moved further. Contrarily, the decoupling point moves toward the higher frequency or the larger wave vector k in the triangular structure and eventually without crossing.
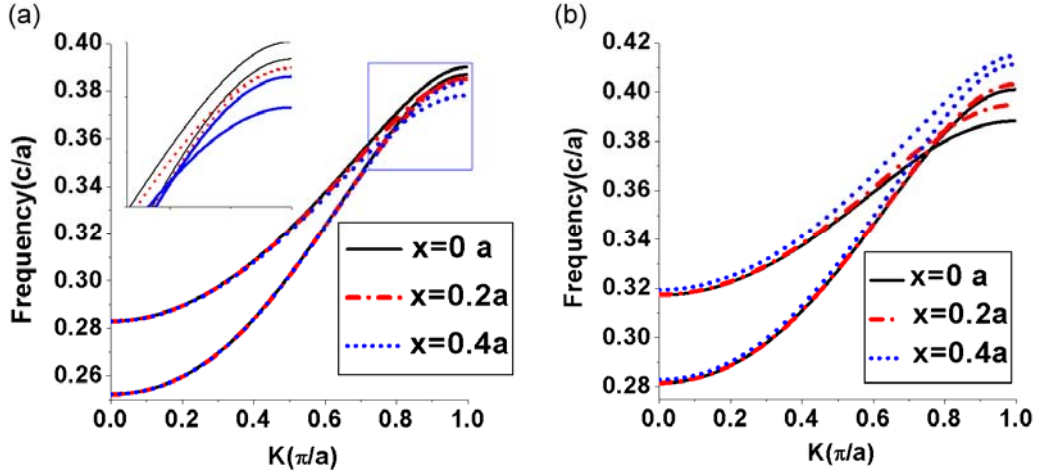
Fig. 18 The dispersion curves as moving the defect rods along the x-direction in the square lattice (a) and triangular lattice (b).

Finally, we used a 2D FDTD method to simulate the electric field transferring between these two shifted coupled PCWs. For the photonic crystal slab, the effective refractive index approach has been proved adequate to reduce this 3D FDTD problem to 2D one [59, 60]. Therefore, 2D FDTD method is sufficient to describe the propagation phenomena in the slab photonic crystal DC, especially for understanding only the physical insight. When an EM wave with the given frequency (0.362 c/a) is incident one (PCW1) of these two channels (or PCWs), the coupling length, for which the energy completely couples to another channel (PCW2), is defined as $\pi/\Delta k$, where Δk is the wave vector mismatch between two modes of the DC at the incident frequency. Using the square lattices as examples, we have shown the dispersion curves of a square lattice DC in Fig. 19(a). Due to rather smaller $\Delta k \sim 0.0346 \, \pi/a$ for the original DC without moving defects, as shown in Fig. 19(b) the coupling length is 29a, which is quite long but finite. When the incident frequency is chosen located at the decoupling point formed by longitudinally shifting all defects a 0.5a distance, the electric field will propagate in the incident channel

without leaking into another channel (see Fig. 19(c)). In addition, moving the line defects close to each other by 0.5*a* makes Δ*k* ~ 0.23 π/*a*, which is a larger vector mismatch, so that the coupling length becomes shorter (~ 4a see Fig. 19(d)). These FDTD simulation results verify the coupling length can be tuned by properly moving the defect rods to shift the decoupling point of dispersion curves that agree with those calculated by PWEM.
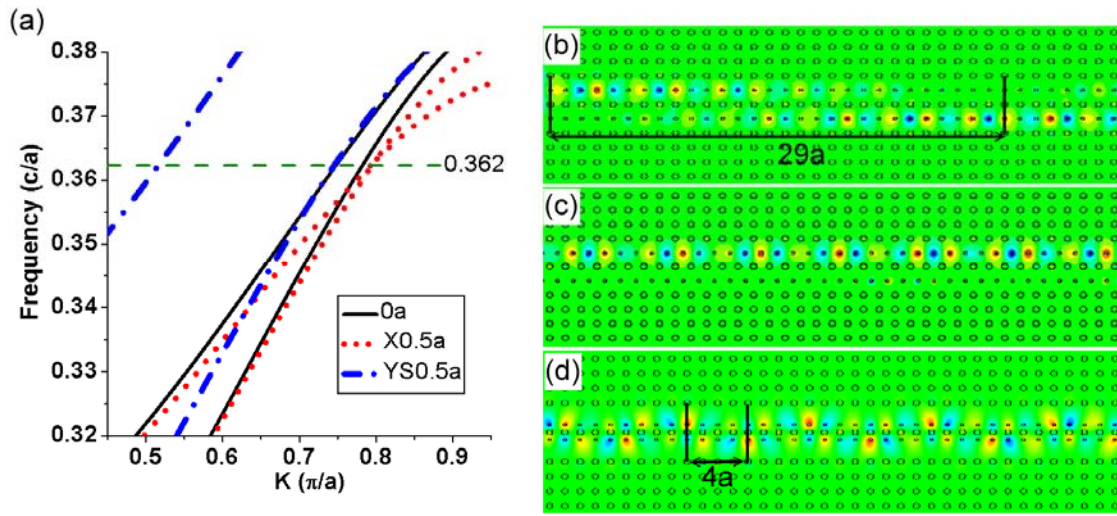
Fig. 19 The dispersion relation curves (a) and the FDTD simulation results of the original DC without moving defects in (b), longitudinally moving the defect rods by 0.5a in (c), and transversely moving the defects closer by 0.5a in (d).

The proposed TBT can also be applied to other structures, e.g., TM polarization in a PC with air holes in a dielectric slab or transversely moving a perfect rod. In the case of a PC with air holes in dielectric slab, the radii of the holes must be increased to insure single mode existing in the PCW and there would be also a decupling point in this structure. On the other hand, the TBT can also well predict the propagation of an EM wave in a single line defect or a DC created by transversely moving a row or two rows of

perfect dielectric rods without changing the radii or dielectric constant of the dielectric rods.

For practical use, the DC can be designed as a dichroic filter for bidirectional multiplexing as reported in [30]. However, it might not realistic to design multichannel filter by cascading DCs with different coupling lengths, because to achieve < 20 dB cross talk, the ratio of coupling lengths of proximal channels has to be less than 0.03. On the other hand, for switching application, we can add a nonlinear medium in the DC to change the refraction index by a controlling light. In the symmetric DC, without the controlling light, the transmission around the decoupling point but not at the decoupling point can be quite high. However, the DC will become asymmetric when the controlling light is injected into one branch of the DC. In this case, the transmission would become very low around the decoupling point [57]. Therefore, the signal can be switch rapidly by a controlling light.
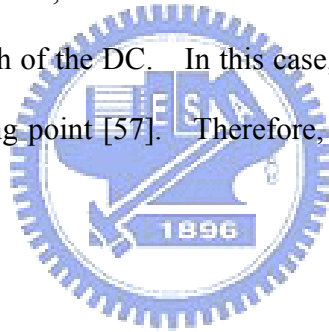
5.3 Summary

The movement of defect rods in the DC is an efficient way to modify its dispersion curves, so that the coupling length and the decoupling point of the DC can be tuned. Moreover, it can make the dispersion curves crossing in the square lattice with a reduced-rods DC. The TBT explains these coupling phenomena consistently with PWEM and FDTD methods and provides design rules for the DC in photonic integrate circuits. The dispersion curves show a blue shift as the defect rods moving away from the center of the PCWs. Two dispersion curves of the DC are pulled apart by reducing the separation of the coupled PCWs, on the contrary, the dispersion curves get closer by enlarging the separation of the coupled PCWs, no matter what the DC is in a square or

triangular structure. However, longitudinally moving the defect rods along waveguides axis, the ratio of the coupling coefficients of the first (α) and the second (β) neighboring rods of the DC would change its magnitude that in turn shifts the decoupling point. This moving effect on the DCs of the square lattice shifts the decoupling point toward the lower frequency or the smaller wave vector k; whereas, toward the higher frequency or the larger wave vector k in the DCs of the triangular lattice.

In this chapter, we focused on the properties of the symmetric couplers. In the next chapter, we will consider the asymmetric cases in which the physical properties are quite different from symmetric ones.

Chapter 6 Physical properties of coupled asymmetric photonic crystal waveguides

From the simulation results by the PWEM for the triangular lattice, the dispersion curves of asymmetric PCWs are not crossing, but the eigenmodes do switch. The electric field ratios of the eigenmodes in both waveguides no longer are ±1, especially at the switching point of the mode pattern (Fig. 21). However, the results of the PWEM or TBT derived from symmetric PCWs cannot provide good reasons to explain these phenomena. Therefore, similar to the tight binding method, we derive an analytic solution considering up to the next nearest-neighbor coupling between two PCWs to describe the physical properties of asymmetric PCWs. This formula provides more generalized discussion and gives a good explanation about asymmetric coupled PCWs. In practice, the coupled identical PCWs should become asymmetric due to the intensity dependent index of refraction in the nonlinear photonic crystal directional coupler, and this can be used as switches to control EM wave to output with proper ratio in each channel.

6.1 Coupled equations of asymmetric photonic crystal waveguides

In Section 2.4, we derived the eigenfrequencies (dispersion relations) and eigenvectors (field amplitudes) of asymmetric PCWs are

$$\omega^\pm(k) = \frac{(\bar{\omega}_1 + \bar{\omega}_2)}{2} \pm \sqrt{\Delta^2 + (g(ka))^2}, \tag{6.1}$$

$$\chi^\pm = (V_0/U_0)^\pm = -\frac{\Delta \pm \sqrt{\Delta^2 + (g(ka))^2}}{g(ka)}, \tag{6.2}$$

where $\Delta = (\bar{\omega}_2 - \bar{\omega}_1)/2$ and $\chi^{\pm}$ are the amplitude ratios corresponding to frequencies $\omega^{\pm}(k)$; $\bar{\omega}_1$ and $\bar{\omega}_2$ are the dispersion relations of the sing PCW1 and PCW2 as shown in Fig. 3; $g(ka) = \alpha + 2\beta Cos(ka)$; α and β are the coupling coefficient between two waveguides.

From the electric field distributions of defects in the square and triangular lattices, shown in Fig. 20, we find that the electric field at the site ($x = 0$, $y = 0$) of the square lattice has the same polarity (sign) as its nearest-neighboring site ($x = 0$, $y = 2a$) and the next nearest-neighboring site ($x = a$, $y = 2a$). Because $\Delta\varepsilon < 0$ for the air-defect PCWs in both square and triangular lattices, the coupling coefficients α and β both are negative values. Here, we assume $\bar{\omega}_2 > \bar{\omega}_1$ in the following discussion; therefore, we shall call the waveguide 2 (waveguide 1) as the high-frequency PCW2 (low-frequency PCW1).
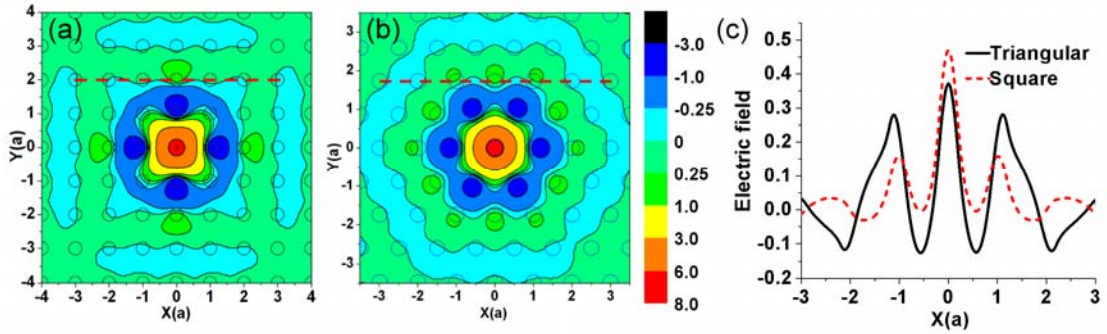
Fig. 20 The electric field distribution (E_z) of a point defect mode in the square lattice for (a) f =0.364 c/a with a reduced-rod (r_d = 0.05a) defect; that in the triangular lattice for (b) eigen frequency f = 0.365 c/a with a defect rod ε_r = 2.56; and (c) The electric field distribution in the dash lines.

Because |g(ka)| has a maximum value at $k = 0$, one should expect that the dispersion curves have the largest splitting there. As α and β are negative values discussed before, $g(ka)$ always is a negative value for all k if $|2\beta/\alpha| < 1$, and its value can change from the negative to the positive sign as k is increasing from 0 to π when $|2\beta/\alpha| > 1$. Under this

condition of $|2\beta/\alpha| > 1$, the coupler can be decoupled when $g(k_D a) = 0$ at a certain $k = k_D$ and have eigenfrequencies $\omega^+ = \bar{\omega}_2$ and $\omega^- = \bar{\omega}_1$ separately; that is, the field launched in PCW1 always will be confined in PCW1 without being coupled to PCW2, and vice versa. We can simply use the ratio of the maximal field values instead of integrals as Eq. (2.9) to estimate coefficients α, β and $|2\beta/\alpha|$ by assuming the field distribution is strongly localized near the dielectric rods. Thus, $|2\beta/\alpha| \sim 2E(0,2a)/E(\pm a,2a)$ in the square lattice and $\sim 2E(0,\sqrt{3}\,a)/E(\pm a,\sqrt{3}\,a)$ in the triangular lattice.

Because $g(ka) < 0$ for $0 \le k < k_D$ under $|2\beta/\alpha| > 1$ (or for all k under $|2\beta/\alpha| < 1$), the lower frequency mode (ω^-) has $-1 < \chi^- < 0$; namely, the eigenmode of the coupler displays the PCW1 and PCW2 electric fields not only being out-of-phase but also concentrated on the low-frequency PCW1. This odd-like fundamental (low-frequency) mode is called the "anti-bonding" mode, borrowed from the molecular physics of two atoms. On the other hand, the high-frequency and even-like mode called the "bonding" mode has $\chi^+ > 1$; thus, it is superimposed by the in-phase electric fields from both PCWs, where the field strength is concentrated on the high-frequency PCW2.

However, as $k > k_D$ under $|2\beta/\alpha| > 1$, $g(ka)$ becomes positive and $0 < \chi^- < 1$. The fundamental mode is a bonding mode, which is superimposed by the in-phase electric fields from both PCWs, where the field strength is concentrated on the low-frequency PCW1. And the high frequency antibonding mode with $\chi^+ < -1$ has the field strength concentrated on the high-frequency PCW2. We find that the fundamental modes of the asymmetric coupler contain no degenerate state (anti-crossing dispersion relations) and can switch from the antibonding to bonding mode as k varies crossing the decoupling point k_D. As the previous study on the symmetric coupler, we simply can set $\Delta = 0$ to

obtain $\chi^{\pm}=\pm 1$ at all k, i.e., the fundamental mode is either odd or even depending upon the sign of $g(ka)$. The dispersion curves of the symmetric coupler can cross at the decoupling point if $|2\beta/\alpha| > 1$. Furthermore, upon increasing the separation of PCWs to two rows apart [27], from Eq. (2.9), coupling coefficients α and β become positive values and are smaller than coupling coefficients of the one-row-separation PCWs. The fundamental mode becomes a bonding mode, and whether or not mode switching would happen still is determined by the criterion: $|2\beta/\alpha| > 1$.

In order to prove that the derived formula by TBT can explain phenomena gotten by PWEM well, we consider for example a 2D triangular (square) lattice PC made by dielectric rods with dielectric constant $\varepsilon_r = 12$ and radius $= 0.2a$ in the air. Due to the field symmetry, the coupling coefficient ratio β/α is a larger value in the triangular lattice than in the square lattice. It should be easier to reach the criterion $|2\beta/\alpha| \approx 2E(0,2a)/E(\pm a,2a) > 1$ of the mode switching behavior in the triangular lattice than in the square lattice, shown in Fig. 20(c). Therefore, we consider a triangular lattice PC, and the line defects forming the PCW1 and PCW2 are created by setting the dielectric constants of defect rods at 2.56 and 2.25, respectively. The eigenfrequencies of a point defect with transverse magnetic field (TM), whose electric field is parallel to the dielectric rods, are $\omega_1 = 0.365$ $(2\pi c/a)$ and $\omega_2 = 0.371$ $(2\pi c/a)$, respectively, where c is the speed of light in vacuum. The decoupling point is located at $k_D = 0.73\pi/a$ where the eigenfrequencies of the PC couplers decouple in the eigenfrequency in single line-defect PCWs, shown in Fig. 21(a). Note that the dispersion curves do not cross in the asymmetric coupler. As shown in Fig. 21(b), the eigenmode of the high (low) frequency band at the wave vectors $k < k_D$ are the bonding (anti-bonding) modes, but these modes switch when $k > k_D$, namely, the eigenmode of high (low) frequency band being

49

anti-bonding (bonding). And the electric field is concentrated on the PCW2 for the high-frequency ($\omega^+(k_D)$) mode and on the PCW1 for the low frequency ($\omega^-(k_D)$) mode at the decoupling point k_D. The mode switching phenomenon at k_D is shown easily by plotting the ratios of the eigenmodes ($\chi=V_0/U_0$) obtained either by the PWEM. We observe that χ's change sign at the decoupling point k_D (see Fig. 21(c)).
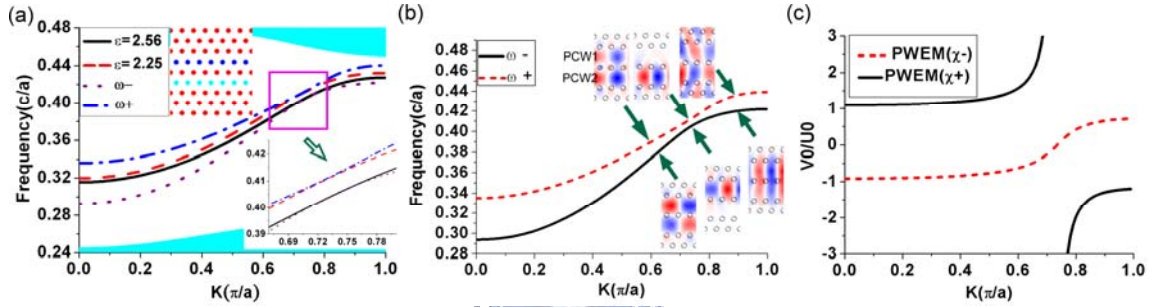
Fig. 21 Simulation results of PWEM. (a) Dispersion relations of two isolated PCWs (ε=2.56 and ε=2.25) and the directional coupler in the triangular lattice (shown as the inset). (b) The dispersion curves of the directional coupler and its eigenmode profiles below, above and at the decoupling point. (c) The mode amplitude ratios of the coupler.

6.2 Electric field distribution and energy transfer

After obtaining the eigenfrequencies (dispersion relations) and eigenvectors (field amplitudes) of the DC, we shall calculate the energy transfer between the coupled PCWs. If an EM wave with a given frequency propagates in the DC, the wave function or field distribution at site n in each of the coupled PCWs can be expressed as the superposition of the eigenmodes of the DC,

$$U_n(na) = Ae^{ik_a na} + Be^{ik_b na} , \tag{6.3}$$

$$V_n(na) = A\chi^a e^{ik_a na} + B\chi^b e^{ik_b na} , \tag{6.4}$$

where the propagation constants of the anti-bonding mode k_a and bonding mode k_b and their corresponding amplitude ratios of χ^a and χ^b can be obtained from Eqs. (6.1) and

(6.2). Note that $\chi^a \chi^b$ is not necessarily equal to -1 for a given frequency because the mode patterns of the DC at a given frequency are not the eigenmodes of the same system. Let $x = na$, one can rewrite Eqs. (6.3) and (6.4) as the following continuous equations,

$$U(x) = Ae^{ik_a x} + Be^{ik_b x} , \qquad (6.5)$$

$$V(x) = A\chi^a e^{ik_a x} + B\chi^b e^{ik_b x} . \qquad (6.6)$$

Taking derivatives of $U(x)$ and $V(x)$ with respect to x, we have the coupled PCW equations

$$\frac{dU(x)}{dx} = iM_1 U(x) + i\kappa_{12} V(x) , \qquad (6.7)$$

$$\frac{dV(x)}{dx} = iM_2 V(x) + i\kappa_{21} U(x) , \qquad (6.8)$$

where $M_1 = \left(k_a\chi^b - k_b\chi^a\right)/\left(\chi^b - \chi^a\right)$ and $M_2 = \left(k_a\chi^a - k_b\chi^b\right)/\left(\chi^a - \chi^b\right)$ are the effective propagation constants of PCW1 and PCW2 of the directional coupler, $\kappa_{21} = -\kappa_{12}\chi^b\chi^a$ and $\kappa_{12} = (k_a - k_b)/(\chi^a - \chi^b)$ are the effective coupling coefficients between PCWs. The solutions of the coupled PCW equations are

$$\begin{bmatrix} U(x) \\ V(x) \end{bmatrix} = \begin{bmatrix} e^{iM_1 x} & 0 \\ 0 & e^{iM_2 x} \end{bmatrix} \begin{bmatrix} D_{11}\eta & iD_{12}\eta \\ iD_{21}\eta^* & D_{22}\eta^* \end{bmatrix} \begin{bmatrix} U(0) \\ V(0) \end{bmatrix}. \qquad (6.9)$$

Here $U(0)$ and $V(0)$ are the electric field amplitudes at $x = 0$, $D_{12} = \left(\kappa_{12} Sin(fx)\right)/f$, $D_{21} = \left(\kappa_{21} Sin(fx)\right)/f$, $D_{11} = D_{22}^* = Cos(fx) - i\delta Sin(fx)/f$, and $\eta = \exp(i\delta x)$, with $f = (k_a - k_b)/2$ and $\delta = f\left(\chi^a + \chi^b\right)/\left(\chi^a - \chi^b\right)$. The maximum energy transferred from PCW1 to PCW2 is proportional to $|\kappa_{21}/f|^2 = 4(\chi^b\chi^a)^2/(\chi^b - \chi^a)^2$ and that from PCW2 to PCW1 is proportional to $|\kappa_{12}/f|^2 = 4/(\chi^b - \chi^a)^2$. There are maximum energy transfers into the other waveguides at $fx=\pi/2$, so coupling length is defined as $\pi/|k_a-k_b|$. There are no crossing points in asymmetric PCWs, as making the coupling would not be infinite by TBT, shown in Fig. 22(a), but the lowest energy transfer still around the

51

decoupling points.   The energy will transfer completely into the other waveguide only in symmetric ones because it happens only at δ=0.
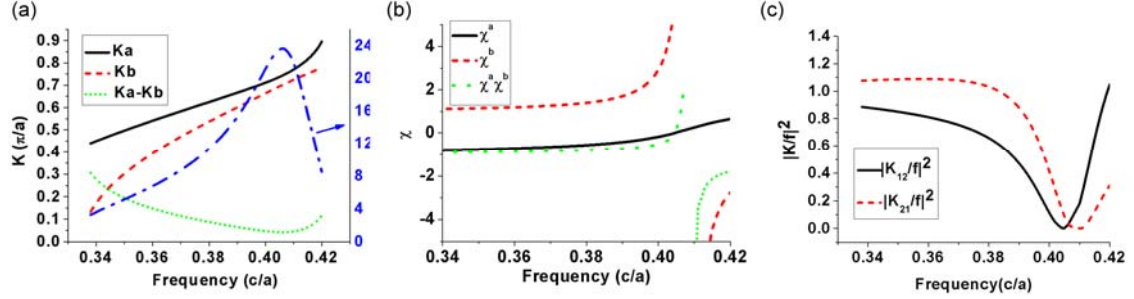

Fig. 22 (a) The wave vectors of the bonding (antibonding) mode and coupling length of the PC couplers for different frequencies. (b) The mode amplitude ratio ($\chi=V_0/U_0$) of the bonding and antibonding mode. (c) The ratios of the maximum energy transferred from the PCW2 to PCW1 ($|k_{12}/f|^2$) and from the PCW1 to PCW2 ($|k_{21}/f|^2$).

For an incident wave frequency ω, the wave vector k_a for the anti-bonding mode should be larger than k_b for the bonding mode for $k < k_D$.   Since $|\chi^a|$ is smaller for large wave vector, if we denote the mode ratio of the lower frequency band at k_b as $\chi^a(k_b)$, we have $|\chi^b \chi^a| \leq |\chi^b \chi^a(k_b)| = 1$ and $4(\chi^b \chi^a)^2 / (\chi^b - \chi^a)^2 \leq 4/(\chi^b - \chi^a)^2$ and ≤ 1, shown in Figs. 22(b) and (c), which are obtained by the PWEM.   Therefore, the maximum energy transferred from PCW1 to PCW2 should be smaller than that transferred from PCW2 to PCW1.   However $|\kappa_{12}/f|^2$ can be larger than 1, meaning the output peak energy can be larger than the input peak energy.   It results from the difference field localization of the eigenmodes.

6.3 Summary

We have extended the TBT to study asymmetric couplings between two non-identical line-defect photonic waveguides.   By considering the coupling between two waveguides

beyond the nearest-neighbor approximation, analytic expressions of the dispersion relations and eigenmode ratios of an asymmetric photonic-crystal coupler agree well with the phenomena calculated by PWEM results. Due to the symmetry breaking, these two dispersion curves will never cross, even with the criterion $|2\beta| > |\alpha|$. Nevertheless, as the symmetric coupler shows, the eigenmode patterns, which are the bonding and anti-bonding modes, do switch on the same dispersion curves when wave vector k varies across the decoupling point. At the higher (lower) frequency of the dispersion relation curve, the electric field distribution of the eigenmodes would localize mainly at the PCW with a higher (lower) eigen frequency, which corresponds to an incomplete EM field transformation between two waveguides. For a given incident frequency, the electric-field distribution and energy transfer of the coupler can be expressed analytically by using the wavevector and derived amplitude ratios of the bonding and anti-bonding modes. The coupling length at the decoupling point no longer is infinite but low energy transfer around there. Although complete energy transfer into the other waveguides is impossible in asymmetric waveguides, the peak power in the output dielectric rods can be larger than that in the input ones due to the electric fields having difference strength of electric field localization in each waveguide.

Chapter 7 Conclusions and Prospective

7.1 Conclusions

In this dissertation, we used TBT to realize the wave propagation of PCWs and CROWs. The basic advantage of this method is that an analytic solution can be derived to describe wave evolution in the waveguides with linear or nonlinear materials. In the single PCW or CROW with Kerr media, we found when a perturbation was superimposed into a plane wave, the perturbation could grow exponentially, as the so-called MI. In the CROWs, the region of MI varies as we change the numbers of separation rods and sign of Kerr media added into the waveguides, but in the MI region, the relationship of nearest-neighbor coupling coefficient (P_1), wave vector of the plane wave (k) and SPM strength must be $P_1\cos(ka)\gamma > 0$ and the MI boundary locates at $ka=\pi/2$. In the air-defect PCWs, the nearest-neighbor coupling coefficient is positive and non-negligible next nearest-neighbor coupling coefficient make the boundary of the MI (ka) exceed $\pi/2$ and exist 2 gain maxima.

If the variation of the envelope of the electric field amplitudes is slow, the incident wave in the MI region could become soliton. From TBT, the soliton propagation criteria of the CROWs and PCWs can be derived. From the criteria, the sign of SPM strength and the 2nd order dispersion (β_2) must have the same sign. As the pulse width of the soliton becomes shorter, the slowly varying amplitude approximation is broken and the pulse will broaden due to high order GVD. As the broadening factor is small, the pulse broadening is dominated by β_3 when ka is away from 0 or π. As ka is near 0 or π, β_3 is almost zero. The pulse broadening is dominated β_4 at soliton propagation condition.

Under this circumstance, the SPM at soliton propagation criteria would be too strong and make the pulse become narrowing at beginning.   When the SPM strength is reduced, the pulse would not be narrowed and the broadening factor would be smaller than that at SPM strength.

When the other identical waveguide is carved into the single PCW with one or several partition rods, we found the crossing point of the dispersion relation curves and coupling length could be tuned by moving the defect rods.   When moving the defect the rods along the propagation direction, the crossing point shifts toward the high frequency or wave vector in triangular lattice PCs and toward the low frequency or wave vector in square lattice PCs.   As moving the two rows of the defect rods in the waveguides close to each other, the coupling length descends and the coupling length ascends as moving two rows of the defect rods away from each other.   These phenomena can be well explained by TBT and coincide with the simulation results of FDTD.

As the other waveguides is not identical to the original one, the symmetry breaks and these two dispersion curves will never cross, even with the criterion $|2\beta| > |\alpha|$.   But the mode switches at this criterion.   At the higher frequency of the dispersion relation curve, the electric field distribution of the eigenmodes would localize mainly at the PCW with a higher eigen frequency and vice versa, which corresponds to an incomplete EM field transformation between two waveguides. For a given incident frequency, the electric-field distributions and energy transfer of the coupler can be expressed analytically by using the wavevector and derived amplitude ratios of the bonding and anti-bonding modes.   The coupling length at the decoupling point no longer is infinite but the lowest energy transfer around there.   Although complete energy transfer into the other waveguides is impossible in asymmetric waveguides, the peak power in the output dielectric rods can be

larger than that in the input ones due to the electric fields having difference strength of electric field localization in each waveguide.

7.2 Prospective

In Chapter 4, we have used EDNLS equation to describe the soliton or pulse propagation in the CROWs or PCWs. In this method, the electric field in the waveguides is assumed as the linear combination of the electric field distribution of the point defect. This is valid when the field propagates in the center of the waveguides, but the field at the input or output boundary must have some distortion, making the EDNLS is not so suitable to describe wave propagation in these regions. In order to consider all circumstance as designing the device, the FDTD method should be used to recheck the results.

In the TBT, only TM polarization is considered because polarization of the electric field is identical in all incident angles of 2D simulation. But as the PC is made of dielectric substrate with air hole pattern, there exists a complete photonic band gap only on TE polarization. We should extend the TBT to TE polarization and compare this analytic result with other numerical results.

In this dissertation, only 2D PCs are considered. To approach the practice experiment devices, we should extend our theory and simulation to the PC slab in which 3D simulation tools should be used. In the primary simulation results of PWEM, we found the dispersion relation curves can cross in PC slab with triangular lattice similar as the simulation results in Chapter 6. We still need to use FDTD to do the double check and get the coupling coefficients from PWEM in order to further analysis the physical properties the PCWs or PC couplers.

References

1. S. G. Johnson, *Photonic crystals : the road from theory to practice* (Kluwer Academic, Boston, 2002).

2. D. W. Prather, S. Y. Shi, J. Murakowski, G. J. Schneider, A. Sharkawy, C. H. Chen, and B. L. Miao, "Photonic crystal structures and applications: Perspective, overview, and development," IEEE J. Sel. Top. Quantum Electron. **12**, 1416-1437 (2006).

3. S. John, "Strong localization of photons on certain disordered dielectric superlattices," Phys. Rev. Lett. **58**, 2486-2488 (1987).

4. E. Yablonovitch, "Inhibited spontaneous emission on solid-state physics and electronics," Phys. Rev. Lett. **58**, 2059-2062 (1987).

5. E. Yablonovitch, "Photonic band-gap crystals," J. Phys. Condens. Matter **5**, 2443-2460 (1993).

6. E. Yablonovitch, "Photonic band-gap structures," J. Opt. Soc. Am. B **10**, 283-295 (1993).

7. C. M. Soukoulis, *Phtonic crystals and light localization in the 21st century* (Kluwer Academic, Dordrecht, The Netherlands, 2000).

8. K. M. Leung, and Y. F. Liu, "Full vector wave calculation of photonic band structures in face-centered-cubic dielectric media," Phys. Rev. Lett. **65**, 2646-2649 (1990).

9. S. G. Johnson, and J. D. Joannopoulos, "Block-iterative frequency-domain methods for Maxwell's equations in a planewave basis," Optics Express **8**, 173-190 (2001).

10. C. E. Reuter, R. M. Joseph, E. T. Thiele, D. S. Katz, and A. Taflove, "Ultrawideband absorbing boundary-condition for terminaiton of wave-guding structures in FD-TD

simulaitons," IEEE Microw. and Guided Wave Lett. **4**, 344-346 (1994).

11. H. Benisty, "Modal analysis of optical guides with two-dimensional photonic band-gap boundaries," J. Appl. Phys. **79**, 7483-7492 (1996).

12. A. Taflove, and S. C. Hagness, *Computational electrodynamics: the finite-difference time-domain method* (Artech House, Norwood, MA, 2000).

13. W. Axmann, and P. Kuchment, "An efficient finite element method for computing spectra of photonic and acoustic band-gap materials - I. Scalar case," J. Comput. Phys **150**, 468-481 (1999).

14. F. Brechet, J. Marcou, D. Pagnoux, and P. Roy, "Complete analysis of the characteristics of propagation into photonic crystal fibers, by the finite element method," Opt. Fiber Technol. **6**, 181-191 (2000).

15. J. B. Pendry, and A. Mackinnon, "Calculation of photon dispersion-relations," Phys. Rev. Lett. **69**, 2772-2775 (1992).

16. K. Sakoda, *Optical properties of photonic crystals* (Berlin, Heidelberg, New York, 2005).

17. A. Yariv, Y. Xu, R. K. Lee, and A. Scherer, "Coupled-resonator optical waveguide: a proposal and analysis," Opt. Lett. **24**, 711-713 (1999).

18. K. Hosomi, and T. Katsuyama, "A dispersion compensator using coupled defects in a photonic crystal," IEEE J. Quantum Electron. **38**, 825-829 (2002).

19. A. Mekis, J. C. Chen, I. Kurland, S. H. Fan, P. R. Villeneuve, and J. D. Joannopoulos, "High transmission through sharp bends in photonic crystal waveguides," Phys. Rev. Lett. **77**, 3787-3790 (1996).

20. C. Ren, J. Tian, S. Feng, H. H. Tao, Y. Z. Liu, K. Ren, Z. Y. Li, B. Y. Cheng, D. Z. Zhang, and H. F. Yang, "High resolution three-port filter in two dimensional photonic

crystal slabs," Opt. Express **14**, 10014-10020 (2006).

21. M. Djavid, and M. S. Abrishamian, "Photonic crystal channel drop filters with mirror cavities," Opt. and Quantum Electron. **39**, 1183-1190 (2007).

22. B. S. Song, T. Asano, and S. Noda, "Recent advances in two-dimensional photonic crystals slab structure: Defect engineering and heterostructure," Nano **2**, 1-13 (2007).

23. S. G. Johnson, C. Manolatou, S. H. Fan, P. R. Villeneuve, J. D. Joannopoulos, and H. A. Haus, "Elimination of cross talk in waveguide intersections," Opt. Lett. **23**, 1855-1857 (1998).

24. P. G. Luan, and K. D. Chang, "Periodic dielectric waveguide beam splitter based on co-directional coupling," Opt. Express **15**, 4536-4545 (2007).

25. M. Djavid, A. Ghaffari, F. Monifi, and M. S. Abrishamian, "Photonic crystal power dividers using L-shaped bend based on ring resonators," J. Opt. Soc. Amer. B **25**, 1231-1235 (2008).

26. A. Chutinan, M. Mochizuki, M. Imada, and S. Noda, "Surface-emitting channel drop filters using single defects in two-dimensional photonic crystal slabs," Appl. Phys. Lett. **79**, 2690-2692 (2001).

27. T. Koponen, A. Huttunen, and P. Torma, "Conditions for waveguide decoupling in square-lattice photonic crystals," J. Appl. Phys. **96**, 4039-4041 (2004).

28. W. Y. Chiu, T. W. Huang, Y. H. Wu, F. H. Huang, Y. J. Chan, C. H. Hou, H. T. Chien, C. C. Chen, S. H. Chen, and J. I. Chyi, "Directional coupler formed by photonic crystal InAlGaAs nanorods," J. Lightw. Technol. **26**, 488-491 (2008).

29. S. Boscolo, M. Midrio, and C. G. Someda, "Coupling and decoupling of electromagnetic waves in parallel 2-D photonic crystal waveguides," IEEE J. Quantum Electron. **38**, 47-53 (2002).

30. F. S. S. Chien, Y. J. Hsu, W. F. Hsieh, and S. C. Cheng, "Dual wavelength demultiplexing by coupling and decoupling of photonic crystal waveguides," Opt. Express **12**, 1119-1125 (2004).

31. F. S. S. Chien, S. C. Cheng, Y. J. Hsu, and W. F. Hsieh, "Dual-band multiplexer/demultiplexer with photonic-crystal-waveguide couplers for bidirectional communications," Opt. Commun. **266**, 592-597 (2006).

32. L. W. Chung, and S. L. Lee, "Photonic crystal-based dual-band demultiplexers on silicon materials," Opt. and Quantum Electron. **39**, 677-686 (2007).

33. T. B. Yu, M. H. Wang, X. Q. Jiang, Q. H. Liao, and J. Y. Yang, "Ultracompact and wideband power splitter based on triple photonic crystal waveguides directional coupler," J. Opt. A, Pure Appl. Opt. **9**, 37-42 (2007).

34. T. Liu, A. R. Zakharian, M. Fallahi, J. V. Moloney, and M. Mansuripur, "Design of a compact photonic-crystal-based polarizing beam splitter," IEEE Photon. Technol. Lett. **17**, 1435-1437 (2005).

35. M. Qiu, and B. Jaskorzynska, "Design of a channel drop filter in a two-dimensional triangular photonic crystal," Appl. Phys. Lett. **83**, 1074-1076 (2003).

36. K. Asakawa, Y. Sugimoto, Y. Watanabe, N. Ozaki, A. Mizutani, Y. Takata, Y. Kitagawa, H. Ishikawa, N. Ikeda, K. Awazu, X. M. Wang, A. Watanabe, S. Nakamura, S. Ohkouchi, K. Inoue, M. Kristensen, O. Sigmund, P. I. Borel, and R. Baets, "Photonic crystal and quantum dot technologies for all-optical switch and logic device," New J. Phys. **8** (2006).

37. D. N. Christodoulides, and N. K. Efremidis, "Discrete temporal solitons along a chain of nonlinear coupled microcavities embedded in photonic crystals," Opt. Lett. **27**, 568-570 (2002).

38. C. H. Huang, Y. H. Lai, S. C. Cheng, and W. F. Hsieh, "Modulation instability in nonlinear coupled resonator optical waveguides and photonic crystal waveguides," Opt. Express **17**, 1299-1307 (2009).

39. C. H. Huang, W. F. Hsieh, and S. C. Cheng, "Tight-binding theory for coupling asymmetric photonic crystal waveguides," in *10th Asia Pacific Physics Conference*(Pohang, SOUTH KOREA, 2007), pp. 1246-1250.

40. C. H. Huang, W. F. Hsieh, and S. C. Cheng, "Physical properties of asymmetric photonic crystal waveguides," J. Opt. A, Pure Appl. Opt. **11**, 015103 (2009).

41. F. S. S. Chien, J. B. Tu, W. F. Hsieh, and S. C. Cheng, "Tight-binding theory for coupled photonic crystal waveguides," Phys. Rev. B **75**, 125113 (2007).

42. A. Imhof, W. L. Vos, R. Sprik, and A. Lagendijk, "Large dispersive effects near the band edges of photonic crystals," Phys. Rev. Lett. **83**, 2942-2945 (1999).

43. W. J. Kim, W. Kuang, and J. D. O'Brien, "Dispersion characteristics of photonic crystal coupled resonator optical waveguides," Opt. Express **11**, 3431-3437 (2003).

44. S. F. Mingaleev, Y. S. Kivshar, and R. A. Sammut, "Long-range interaction and nonlinear localized modes in photonic crystal waveguides," Phys. Rev. E **62**, 5777-5782 (2000).

45. S. F. Mingaleev, and Y. S. Kivshar, "Self-trapping and stable localized modes in nonlinear photonic crystals," Phys. Rev. Lett. **86**, 5474-5477 (2001).

46. S. F. Mingaleev, A. E. Miroshnichenko, Y. S. Kivshar, and K. Busch, "All-optical switching, bistability, and slow-light transmission in photonic crystal waveguide-resonator structures," Phys. Rev. E **74**, 046603 (2006).

47. A. G. Shagalov, "Modulational instability of nonlinear waves in the range of zero dispersion," Phys. Lett. A **239**, 41-45 (1998).

48. L. Hadzievski, M. Stepic, and M. M. Skoric, "Modulation instability in two-dimensional nonlinear Schrodinger lattice models with dispersion and long-range interactions," Phys. Rev. B **68**, 014305 (2003).

49. F. K. Abdullaev, A. Bouketir, A. Messikh, and B. A. Umarov, "Modulational instability and discrete breathers in the discrete cubic-quintic nonlinear Schrodinger equation," Physica D-Nonlinear Phenomena **232**, 54-61 (2007).

50. F. M. Mitschke, and L. F. Mollenauer, "Discovery of the soliton self-frequency shift," Opt. Lett. **11**, 659-661 (1986).

51. T. Kamalakis, and T. Sphicopoulos, "Analytical expressions for the resonant frequencies and modal fields of finite coupled optical cavity chains," IEEE J. Quantum Electron. **41**, 1419-1425 (2005).

52. S. Mookherjea, "Dispersion characteristics of coupled-resonator optical waveguides," Opt. Lett. **30**, 2406-2408 (2005).

53. I. Neokosmidis, T. Kamalakis, and T. Sphicopoulos, "Optical delay lines based on soliton propagation in photonic crystal coupled resonator optical waveguides," IEEE J. Quantum Electron. **43**, 560-567 (2007).

54. Y. S. Kivshar, and G. P. Agrawal, *Optical solitons* (Academic, California, 2003).

55. G. P. Agrawal, *Nonlinear fiber optics* (Academic, Burlington, MA, 2007).

56. C. H. Huang, W. F. Hsieh, and S. C. Cheng, "Tuning the decoupling point of a photonic-crystal directional coupler," J. Opt. Soc. Amer. B **26**, 203-209 (2009).

57. C. H. Huang, W. F. Hsieh, and S. C. Cheng, "Tight-binding theory for coupling asymmetric photonic crystal waveguides," J. Korean Phys. Soc. **53**, 1246-1250 (2008).

58. J. D. Joannopoulos, S. G. Johnson, J. N. Winn, and R. D. Meade, *Photonic crystals*

(Princeton University Press, New Jersey, 2008).

59. M. Qiu, "Effective index method for heterostructure-slab-waveguide-based two-dimensional photonic crystals," Appl. Phys. Lett. **81**, 1163-1165 (2002).

60. W. D. Zhou, Z. X. Qiang, and L. Chen, "Photonic crystal defect mode cavity modelling: a phenomenological dimensional reduction approach," J. Phys. D **40**, 2615-2623 (2007).

黃至賢簡歷(Vita)

基本資料:

姓名: 黃至賢 (Chih-Hsien Huang)

性別: 男

出生年月日: 1974 年 10 月 03 日

出生地: 彰化縣

永久通訊處: 彰化縣伸港鄉新港村忠孝路 44 號

Email: hjames.eo90g@nctu.edu.tw

hjameseo90g@hotmail.com

學歷:

1993.9-1998.6 國立台灣師範大學物理系學士

2001.9-2003.6 國立交通大學光電工程研究所碩士

2004.9-2009.6 國立交通大學光電工程研究所博士

博士論文題目:

緊束縛理論在光子晶體波導的應用

Tight Binding Theory for Photonic Crystal Waveguides

Publication list

Journal paper

1. <u>C. H. Huang</u>, W. F. Hsieh, and S. C. Cheng, "Tight-binding theory for coupling asymmetric photonic crystal waveguides," J. Korean Phys. Soc. **53**, 1246-1250 (2008).

2. <u>C. H. Huang</u>, W. F. Hsieh, and S. C. Cheng, "Tuning the decoupling point of a photonic-crystal directional coupler," J. Opt. Soc. Amer. B **26**, 203-209 (2009).

3. <u>C. H. Huang</u>, W. F. Hsieh, and S. C. Cheng, "Physical properties of asymmetric photonic crystal waveguides," J. Opt. A, Pure Appl. Opt. **11**, 015103 (2009).

4. <u>C. H. Huang</u>, Y. H. Lai, S. C. Cheng, and W. F. Hsieh, "Modulation instability in nonlinear coupled resonator optical waveguides and photonic crystal waveguides," Opt. Express **17**, 1299-1307 (2009).
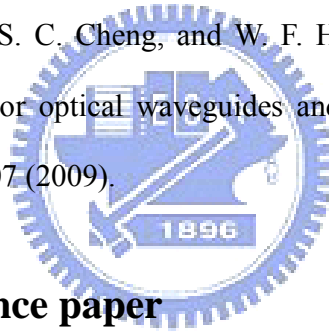
International conference paper

1. <u>C. H. Huang</u>, W. F. Hsieh, and S. C. Cheng, "Coupling theory of asymmetric photonic-crystal waveguides," in *Progress in Electromagnetics Research Symposium (PIERS 2008)*(Cambridge, MA, 2008), pp. 187-191.